Received: 17 July 2024 | Revised: 17 October 2024 | Accepted: 6 December 2024

DOI: 10.1111/jace.20343

Journal of the American Ceramic Society

RESEARCH ARTICLE

The light detection performance of ZnO-based Schottky-type photodetector as a function of changing solution molarity

Mehmet Erkol[1] | **Mustafa Coşkun**[2,3] | **Fatih Mehmet Coşkun**[2,3] | **Adem Kocyigit**[4]

[1]Department of Science Teaching, Education Faculty, Afyon Kocatepe University, Afyon, Turkey

[2]Department of Engineering Physics, Faculty of Engineering and Natural Sciences, Istanbul Medeniyet University, Uskudar, Istanbul, Turkey

[3]Istanbul Medeniyet University Science and Advanced Technology Research Center (IMU-BILTAM), Istanbul, Turkey

[4]Department of Electronics and Automation, Vocational High School, Bilecik Seyh Edebali University, Bilecik, Turkey

Correspondence
Mehmet Erkol, Department of Science Teaching, Education Faculty, Afyon Kocatepe University, Afyon 03200, Türkiye.
Email: merkol@aku.edu.tr

Adem Kocyigit, Department of Electronics and Automation, Vocational High School, Bilecik Seyh Edebali University, Bilecik 11000, Türkiye.
Email: adem.kocyigit@bilecik.edu.tr

Abstract

Wide band gap metal oxides can increase the detection band and performance of photodetectors. Among them, zinc oxide (ZnO) is a multi-functional oxide metal with various applications in various areas, that is, gas sensors, electronics, and optoelectronics. In this study, we employed ZnO metal oxide layers, which were synthesized by hydrothermal method, as interfacial layers for Schottky-type silicon-based photodetectors between Au metal and p-Si with 46 and 56 mM ZnO solution molarities to fabricate Au/ZnO/p-Si heterostructures. Synthesized ZnO morphology and crystallinity were tested by scanning electron microscopy and x-ray diffraction techniques. The Au/ZnO/p-Si heterostructures were investigated for photodetector applications by current–voltage (*I–V*) analysis in various light densities ranging from dark to 150 mW/cm^2, and different wavelengths for the same light irradiance power. *I–V* characteristics under dark and light situations were used to extract diode characteristics and light detection parameters. The impedance analysis technique was also employed to demonstrate the capacitance behavior for the Au/ZnO/p-Si heterostructures. The obtained Au/ZnO/p-Si heterostructures confirms that trap levels are important to obtain high-performance photodetectors.

KEYWORDS
flower-like structures, hydrothermal method, photodetector, ZnO

1 | INTRODUCTION

Metal oxides compose an oxide anion and metal cation, and they can be used variety of applications, that is, gas sensors, film coatings, solar cells, and energy storage applications.[1–3] Among the metal oxides, ZnO is well-studied and a well-known material and environmentally friendly. It has a wide band gap of 3.3 eV and a large exciton binding energy of 60 meV.[4] These behaviors make it a good candidate for many applications such as catalysis, sunscreen coatings, electronics, solar cells, gas sensors, and photodetectors with various structures.[5–9] ZnO structures can be synthesized by various techniques like sol-gel, hydrothermal, spray pyrolysis, solvothermal, and atomic layer deposition.[10–13] The hydrothermal method has several advantages such as green chemistry synthesis, high purity and homogeneity, energy efficiency, and costs, to obtain easily complex structures among these methods.[14] ZnO can be synthesized by hydrothermal method with various structural shapes under different reaction conditions.[15] Thus, the physical properties of a device can be controlled in that way by ZnO structures.

Semiconductor technology is very important in our modern life and composes daily electronic devices from

basic sensors and chips to smartphones and high-speed computers.[16,17] The adjustable electric conductivity, miniaturization, efficiency, and fast switching behaviors make semiconductors favorable materials for a wide range of applications from electronics to optoelectronics.[18] Optoelectronic devices include LEDs, photodetectors, solar cells, and many others. One of them, photodetectors, is capable of light detection by producing electron and hole pairs (exciton) when photons strike them.[19] Thus, the produced excitons are driven by an internal force such as an electric field or barrier potential to the different poles to produce a signal.[20] Photodetectors have applications in telecommunication, sensors, and imaging.[21] PIN, avalanche, and Schottky are various types of photodetectors, and among them, Schottky photodetectors are constructed by joining a semiconductor and a metal together, and the barrier height between them operates as a driving force for holes and electrons.[22,23] The electron-hole pairs are created inside the semiconductor when high-energy light photons hit the structure. The Schottky barrier separates these carriers to the different poles.[24] This separation causes an electrical current to flow through the device, which the light can subsequently be sensed, and the device is used for a variety of usage areas.[25] They are also suitable for radio frequency and microwave applications because of their fast response and small capacity.[26]

The photodetectors have some drawbacks such as increasing dark current by increasing temperature, high dark current, small active area, and applied voltage for triggering.[27] The internal defects or dislocations can decrease the performance of the photodetectors because of making trap levels in the band gap of the semiconductor as non-radiative recombination centers.[28] To reduce the concentration of interfacial trap states and enhance the probability of collecting the excess carriers (i.e., electrons and holes), rather than losing them through non-radiative Shockley–Read–Hall recombination, researchers have sometimes used an interlayer such as metal oxides, polymers, or insulator films in Schottky photodetectors.[29–32] There are many studies in the literature about ZnO-based photodetectors.[33] However, there is not much study on the changing molarity-based ZnO interfacial layered Schottky-type photodetector according to our best knowledge. In this study, we easily synthesized ZnO flower-like structures by a hydrothermal route for their use in Schottky-type photodetector devices as an interlayer and investigated the electrical properties of Au/ZnO/p-Si heterostructures by 46 and 56 mM solution molarities under varying irradiance levels and different wavelengths as well as impedance spectroscopy technique.

2 | EXPERIMENTAL PROCEDURES

Zinc chloride ($ZnCl_2$) was employed as precursor for the synthesis of ZnO flowers by the hydrothermal method as described in Ref [34]. The different amounts of $ZnCl_2$ were dissolved in distilled water by stirring 2 h, and the solution pH was adjusted to 9 for by including triethylamine. The solution was autoclaved at 200°C for 2 h after being stirred for 24 h. To obtain the ZnO interlayer on the polished side of a p-Si substrate, ZnO nanostructures synthesized at 46 and 56 mM zinc concentrations were dispersed in methanol. The employed substrate, which had 10 Ω cm resistivity and 7.3×10^{15} cm^{-3} carrier concentration, was cut into 2 cm^2 slices and cleaned by an ultrasonic cleaner in distilled water, acetone, and isopropanol. The cleaned pieces were then moved to a thermal evaporation system after removing unwanted oxide layer from the surfaces with HF:H_2O mixture (1:10) to achieve Al back contact on the back side of the pieces. An annealing process at 500°C was employed on the p-Si/Al with a furnace in N_2 medium for 3 min to create ohmic contact. The dispersed ZnO solutions were deposited on the p-Si/Al to obtain ZnO interfacial layer. Finally, to construct the Au/ZnO/p-Si heterostructures, Au metal contacts were evaporated on the ZnO interfacial layers. The resulting schematic of the photodetector and the measuring medium can be found everywhere.[35–37] Three different devices were fabricated for 46 and 56 mM solution molarity conditions for repeatability of the devices.

X-ray diffraction (XRD) patterns were recorded by the PANalytical Empyrean x-ray diffractometer of from 10° to 60°. Morphological visions of the ZnO samples were taken via the scanning electron microscope (SEM) of FEI QUANTA FEG 450 brand. A Sciencetech solar simulator was utilized to expose light on Au/ZnO/p-Si photodetector at a variety of wavelengths and AM 1.5G for various power irradiance levels. A picoammeter/voltage sourcemeter of Keithley 2400 was employed to record the *I–V* data. Capacitance–voltage (*C–V*) data were collected by HP 4192A LF Impedance Analyzer.

3 | RESULTS AND DISCUSSION

To elucidate the morphology and structure types of the hydrothermally synthesized ZnO structures, SEM images were taken for various magnifications and different places on the surfaces of ZnO interlayers. SEM images of the ZnO structures with 46 and 56 mM solution molarities for different magnifications are shown in Figures 1A–D and 2A–D, respectively. The ZnO surfaces are almost uniform and show flower-like granular structures in higher

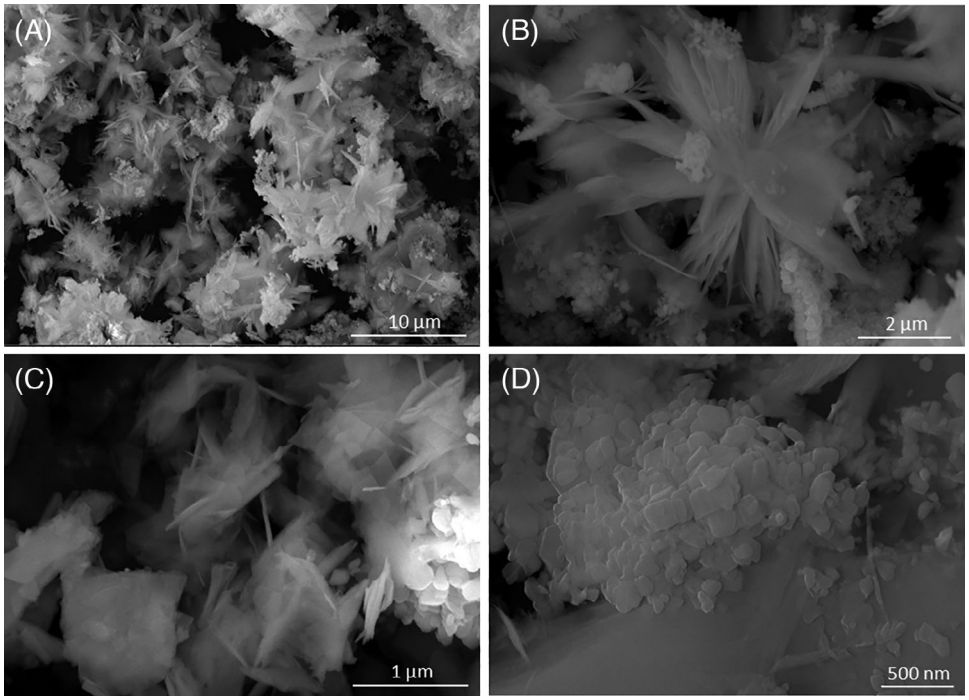

FIGURE 1 Scanning electron microscope (SEM) images of ZnO samples with 46 mM solution molarity for (A) 15 000×, (B) 40 000×, (C) 100 000×, and (D) 120 000× magnifications.

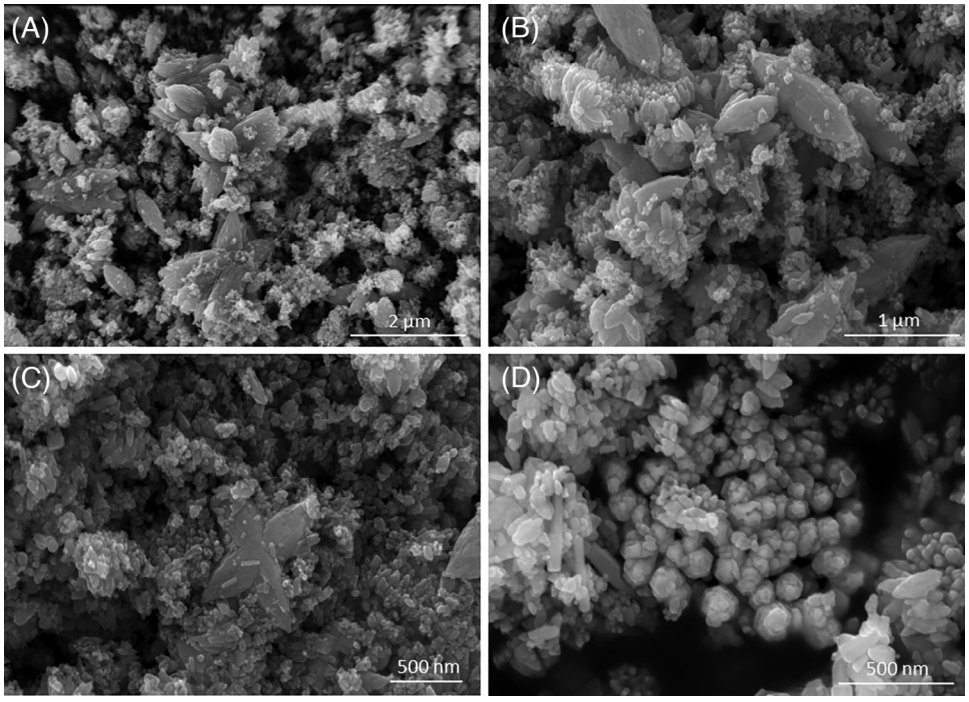

FIGURE 2 Scanning electron microscope (SEM) images of ZnO samples with 56 mM solution molarity for (A) 50 000×, (B) 100 000×, (C) 120 000×, and (D) 200 000× magnifications.

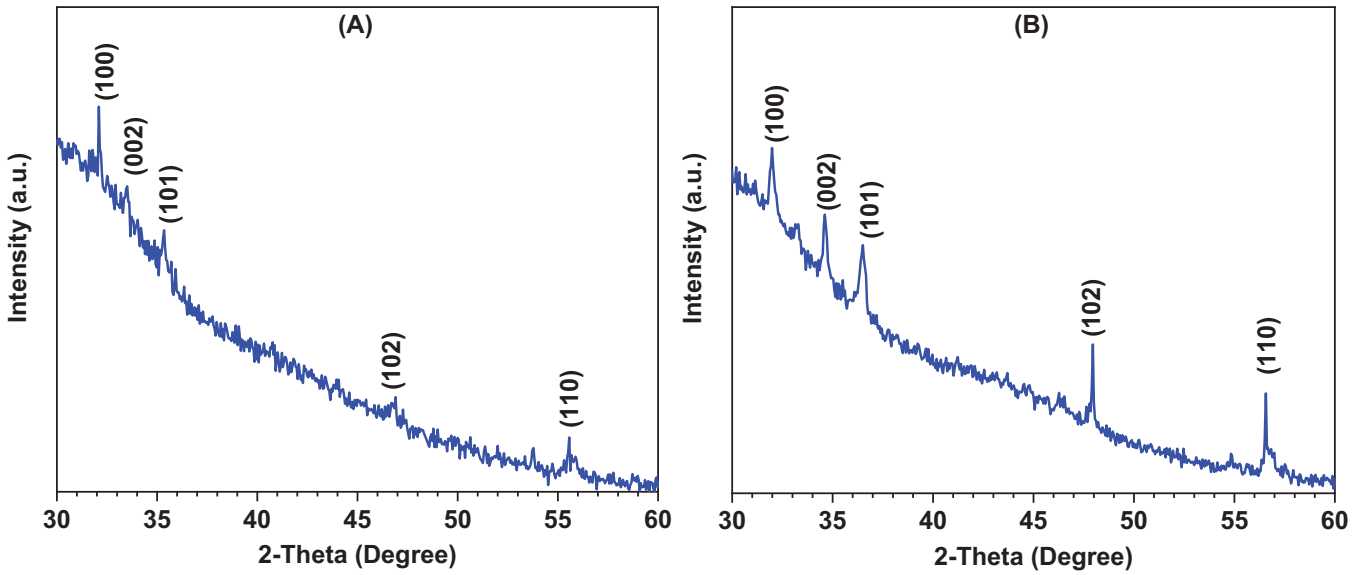

FIGURE 3 X-ray diffraction (XRD) patterns of ZnO interlayers of (A) 46 mM and (B) 56 mM solution molarities.

magnification in the case of lower molarity. However, this granulation increased by increasing the molarity of ZnO. Furthermore, as can be seen from the high-magnification SEM photographs given in Figure 1D, nanoflakes merged during the reaction process to form nanoflower structures. The structure of the nanoflakes of ZnO or porous surfaces for Si as much as possible increases the light interaction and provides more photon absorption according to flat surfaces of ZnO and Si wafers according to the literature.[38,39] Furthermore, the combination of these flakes to form flower-like structures may increase this potential. In Figure 2A–D, as a result of increasing ZnO molarity, the formation of irregular and relatively larger nanoparticles was observed, indicating a lower surface area compared to Figure 1. Therefore, ZnO nanoflower structures can increase the light absorption rate and charge transfer properties of electronic devices.[40] Good photodiode characteristics such as high responsivity and specific detectivity of the photodiode can be obtained based on synthesized ZnO nanostructures such as flower, rod, and thin film.[41–43] Thus, flower-like structures can help to increase the performance of the photodetector.

To confirm the crystalline nature of the synthesized ZnO flavor-like structures, XRD measurements were conducted on the ZnO interlayer films. XRD patterns of ZnO structures, which were obtained from the 46 and 56 mM solutions molarities, have been displayed in Figure 3A,B for the two-theta degrees from 10 to 60, respectively. The pattern revealed that ZnO exhibited (1 0 0), (0 0 2), (1 0 1), (1 0 2), and (1 1 0) planes with hexagonal wurtzite crystalline structure, and they were found to be consistent with the JCPDS No. 36-1451 cards.[44] The characteristics peaks observed for the ZnO crystal structure demonstrated that the ZnO structures were synthesized in a manner consistent with a crystalline structure, with no evidence of the presence of additional compounds in the form of second-phase peaks. The XRD peak intensities are high for higher molarity solution of 56 mM, and this can be ascribed to the increment in the molarity making it to deposit of ZnO structure amount on the p-Si.[45]

The constructed Au/ZnO/p-Si heterostructures for different molarities of ZnO solutions have been investigated by performing *I–V* analysis under both dark and varying conditions of irradiance levels from 10 to 150 mW/cm^2. The *I–V* curves of the Au/ZnO/p-Si heterostructures for dark conditions are shown in Figure 4A,C for 46 and 56 mM ZnO solution molarities, respectively. The Au/ZnO/p-Si heterostructures revealed typical Schottky diode behavior blocking current at reverse bias at the level from μA to nA and passing current at forward bias after a threshold voltage of about 0.300–0.400 V.[46] *I–V* curve of the Au/ZnO/p-Si for changing irradiance levels as a function has been displayed in Figure 4B,D for 46 and 56 mM ZnO solution molarities, respectively. When the 10 mW/cm^2 irradiance level hit the Au/ZnO/p-Si, both heterostructures and electron-hole pairs occurred, and the current immediately increased 3- or 5-fold at negative voltages. This increase confirms the photodetection behavior of the Au/ZnO/p-Si heterostructure. Li et al. fabricated p-Si/MoS_2 heterostructures and confirmed the same detection behavior by obtaining electron-hole pairs.[47] After the 10 mW/cm^2 irradiance level, the increase of the current slowed down for periodic increases at each irradiance. This case may depend on the saturation of the current with recombination mechanism or interfacial traps due to different types of current conduction mechanisms.[48] Furthermore,

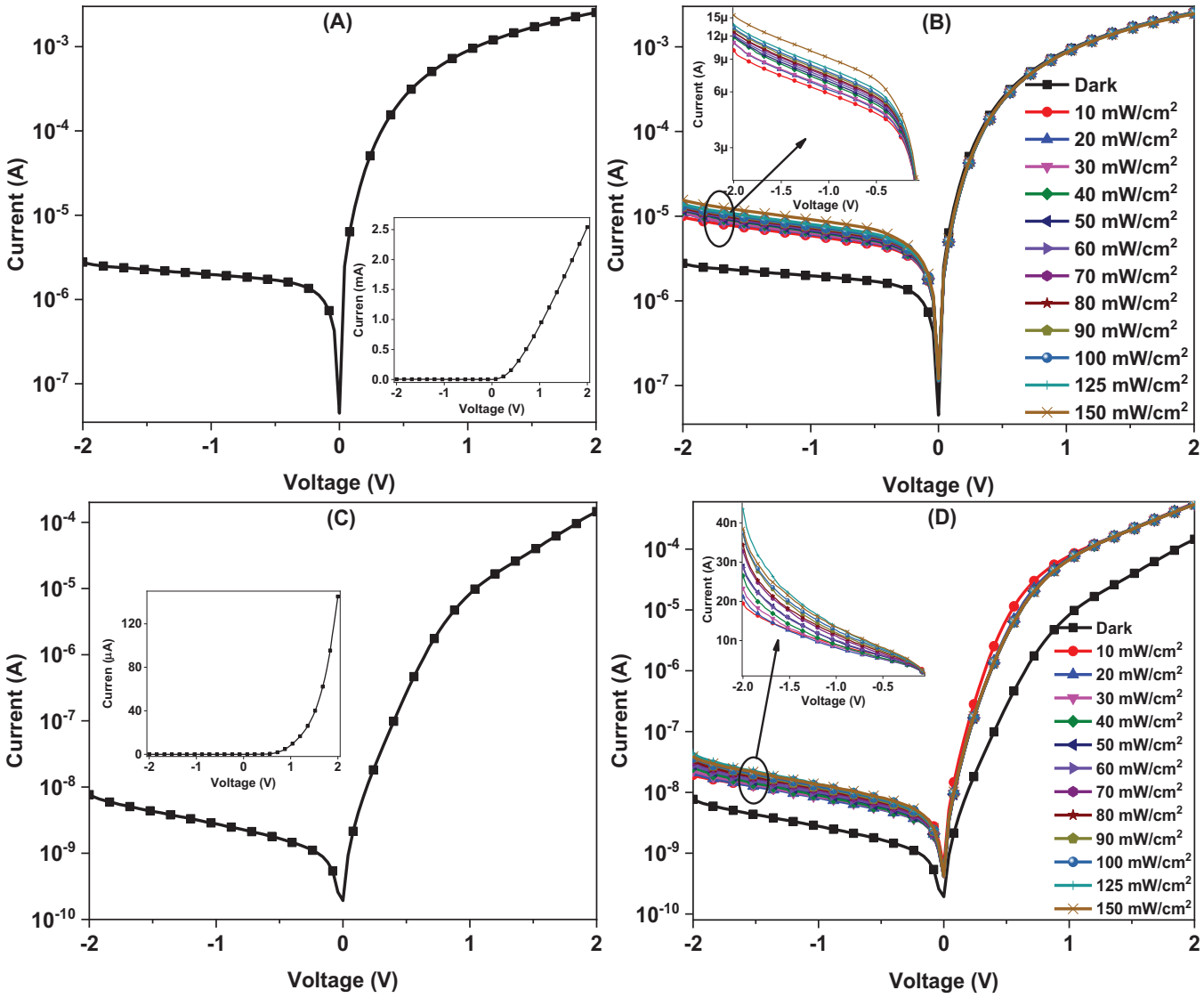

FIGURE 4 Parts (A) and (C) display dark condition, (B) and (D) irradiance levels-dependent profile *I–V* characteristics of Au/ZnO/p-Si heterostructures for 46 and 56 mM solution molarity conditions, respectively.

increasing the molarity of the solution caused to decrease at reverse current and saturation current from μA to nA level because the ZnO interlayer may be induced to decrease the conductivity of the Au/ZnO/p-Si heterostructure.

To better understand the current conduction mechanism in the Au/ZnO/p-Si heterostructure, various parameters such as series resistance (R_s), ideality factor (n), and barrier height (Φ_b) values are extracted with the methods of thermionic emission theory (TE), Cheung or Norde methods from the *I–V* characteristics.[37,49] In the literature, the detailed analysis of these methods for diode parameters has been explained in the case of determination and formulation.[50–52] The values of the n and the Φ_b of the Au/ZnO/p-Si heterostructures have been computed by the *I–V* curve according to the TE theory in the dark and under different illumination conditions with different irradiance levels. Figure 5A,C shows the variation of n and the Φ_b profiles of the Au/ZnO/p-Si heterostructures as a function of irradiance levels for 46 mM and 56 mM solution molarities, respectively. Although the Φ_b was found to be 0.612 eV, the n was determined to be 2.152 in dark condition for 46 mM solution molarity, and they obtained 0.826 eV and 2.085 for 56 mM ZnO solution. In the case of 46 mM solution, the Φ_b values decreased slowly from 0.612 to 0.608 eV for all ranges of irradiance levels, and the n values increased from 2.152 to 2.322 for 10 mW/cm^2, then increased linearly from 2.381. For 56 mM solution, the Φ_b values decreased fast from 0.826 to 0.758 eV, and the n values rose from 2.085 to 2.569 for up to 30 mW/cm^2, then stayed constant toward higher irradiance levels. Such variations at the n and the Φ_b by increment of irradiance level may be due to

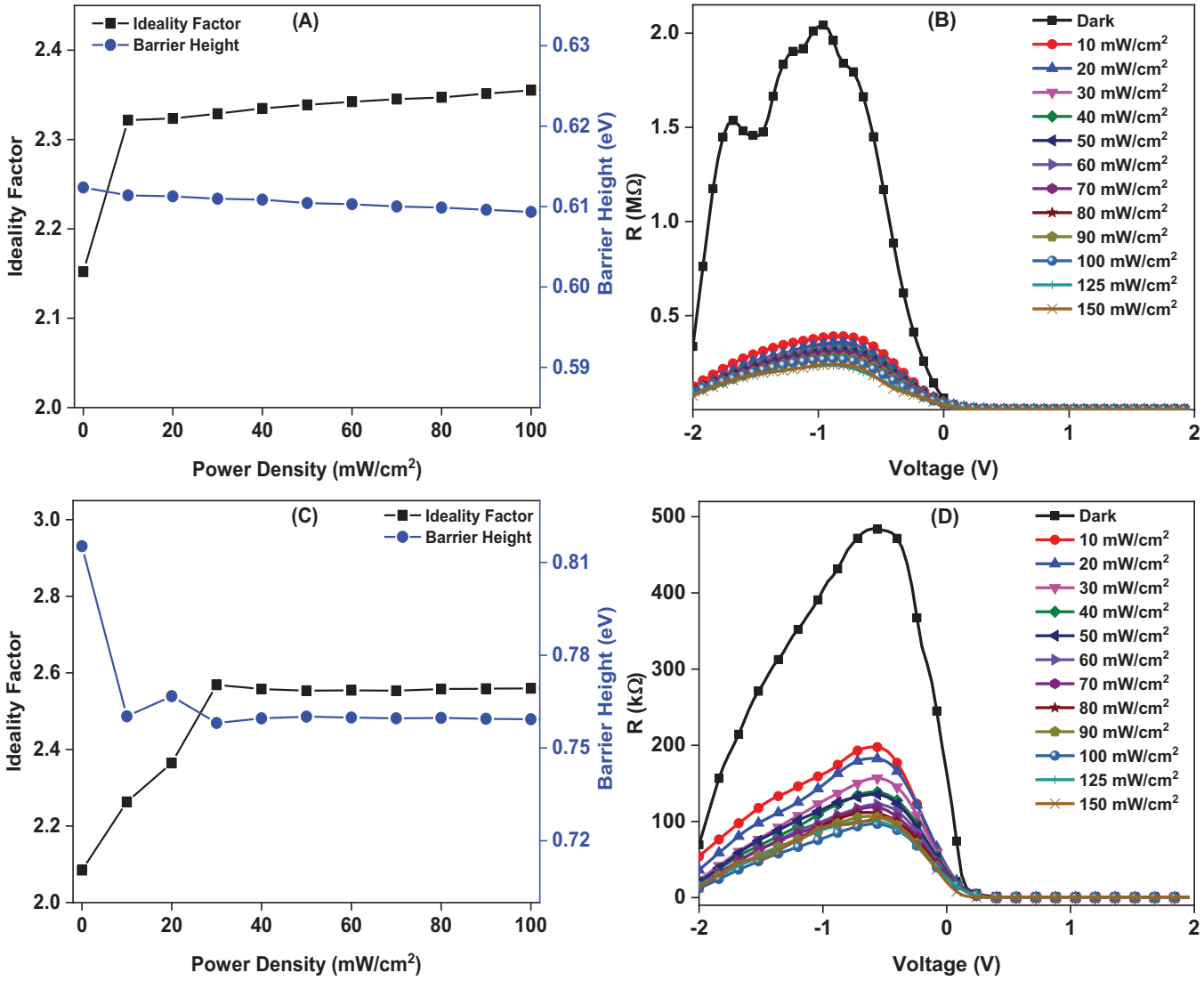

FIGURE 5 Parts (A) and (C) show n and Φ_b changes, (B) and (D) R_j–V curve of the Au/ZnO/p-Si by varying irradiance levels for 46 and 56 mM solution molarity conditions, respectively.

barrier inhomogeneity or electron tunneling out of the barrier with higher energy.[53] The slight changes in the current by variation of the irradiance levels at forward biases imply that the Au/ZnO/p-Si heterostructures have less barrier inhomogeneity. This is important for high-performance photodevices.[54]

To achieve low noise equivalent power or a high signal-noise ratio, the shunt (R_{sh}) and series resistance (R_s) of a photodetector are important parameters. They are derived from the junction resistance (R_j), which is obtained by dV/dI formalism, at reverse bias for R_{sh} and forward biases for R_s.[55] Figure 5B,D shows the R_j–V curves of the Au/ZnO/p-Si heterostructures for different irradiance levels in the case of 46 and 56 mM solution molarity conditions, respectively. The R_{sh} value of the Au/ZnO/p-Si with 46 mM solution for the dark is about 10^7 Ω and it is about 10^9 Ω level for Au/ZnO/p-Si with 56 mM solution. However, although the R_{sh} values decrease to the level of 10^3 owing to the charge carriers increase with the increase of the irradiance levels for 46 mM molarity, they decrease to 10^5 Ω level for 56 mM solution. This decrease with increasing irradiance levels can be depended on that Au/ZnO/p-Si heterostructures can give a response change of power level and exhibit photodetector behavior. The R_s values of the devices for 46 and 56 mM solution molarity are the level of 10^3 Ω.

To confirm the values determined from the TE theory, the parameters of the diodes can be accounted for using the Norde and Cheung methods. The equation for the calculation and the detailed explanation of how to figure out of the parameters using these techniques can be referred to the literature.[56,57] It is possible to compute the Φ_b and R_s values by the $F(V)$ graph of the Norde function. This method uses the $F(V)$ minimum value, the associated voltage minimum,

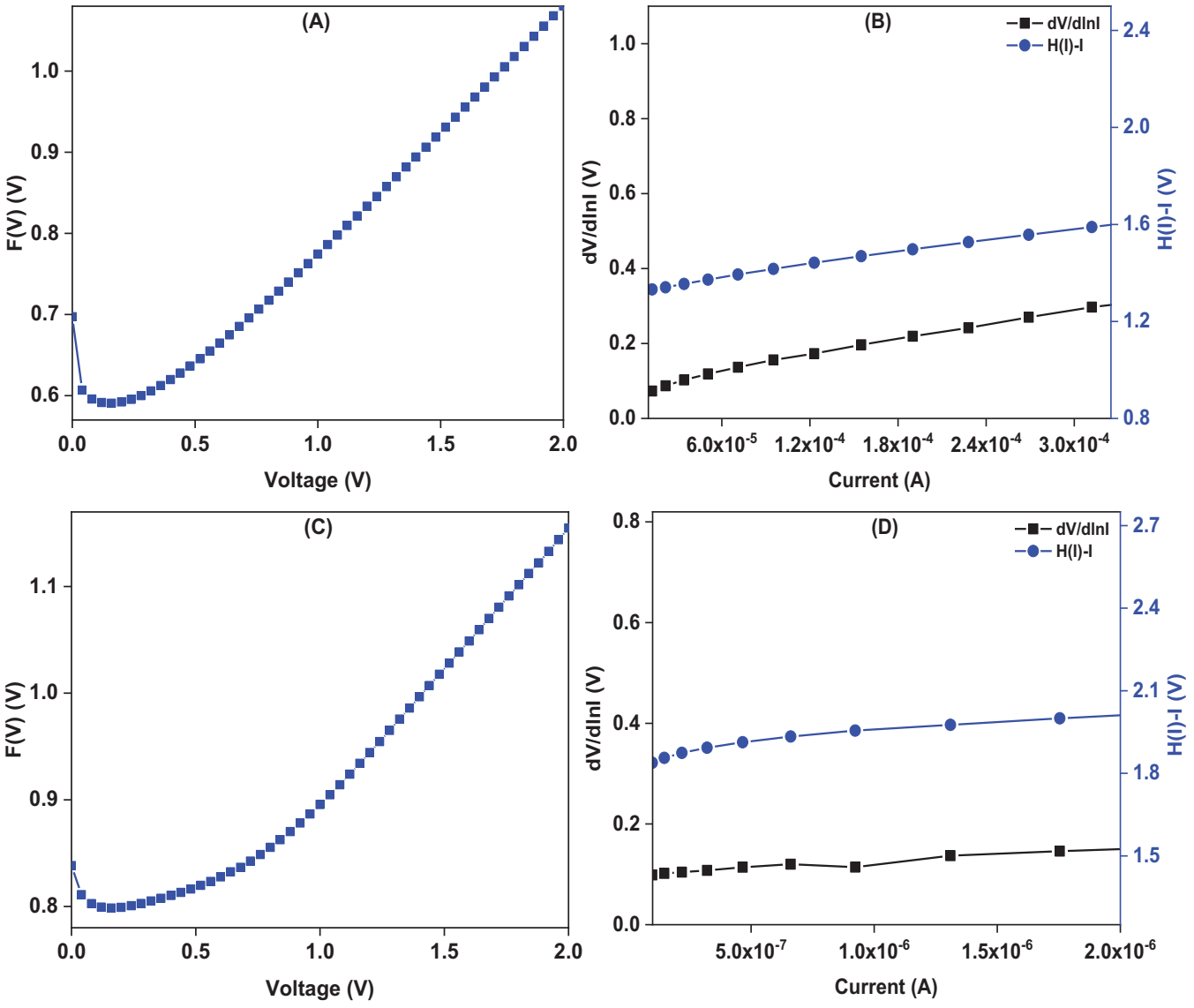

FIGURE 6 Parts (A) and (C) present Norde plots, (B) and (D) show Cheung plots of the Au/ZnO/p-Si heterostructures with 46 and 56 mM solution molarities at dark situation, respectively.

and current values to determine the Φ_b and R_s. Figure 6A,C presents the *F(V)* versus *V* plots of the Au/ZnO/p-Si heterostructures for the dark environment, and they display normal Norde function plots 46 and 56 mM solution molarity conditions. The series resistance was found as 1.012 kΩ, whereas the Φ_b was found to be 0.618 eV for 46 mM solution molarity. They were obtained as 3.349 MΩ and 0.826 eV for 56 mM solution molarity. Higher R_s and Φ_b values at the 56 mM ZnO solution molarity-based heterostructure than the heterostructure with 46 mM solution molarity can be ascribed to the dielectric behavior of ZnO.

The n, Φ_b, and two alternative R_s values are also derived using the Cheung technique by plotting the *dV/dlnI* and *H(I)* functions against the current. Although the n and Φ_b values are determined by y-intercepts of the dV/dln$I$ and $H(I)$ functions, their slopes of two different close R_s values. Figure 6B,D presents Cheung's curve graphs of the Au/ZnO/p-Si for 46 and 56 mM solution molarity conditions in the dark state, and the plots show almost straight-line characteristics concerning the current. The n and Φ_b values were accounted to be 2.199 and 0.601 eV, respectively, whereas the R_s values were determined as 1.164 and 1.071 kΩ from dV/dln$I$ and $H(I)$ plots for 46 mM solution molarity. Although the n and Φ_b values were determined to be 2.126 and 0.810 eV, the R_s values were obtained to be 3.892 and 3.075 MΩ for 56 mM ZnO solution molarity. Whereas the adjacent values of the R_s affirm the consistency of the Cheung technique, the different results for all methods and all values can be linked to the approach of the *I–V* curve.[58]

The ratio of the forward and reverse bias currents for a fixed voltage is called the rectification ratio (*RR*). It gives

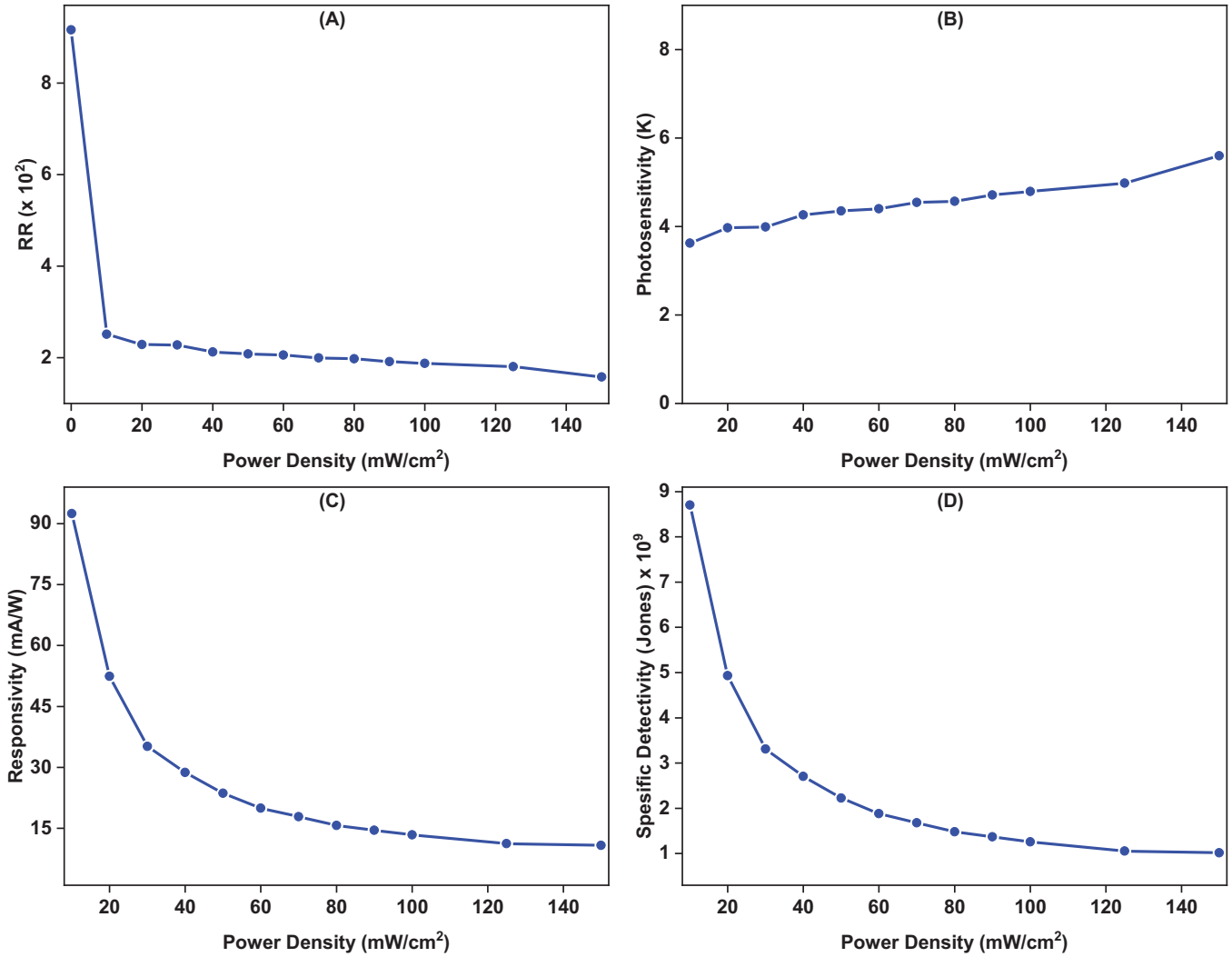

FIGURE 7 Parameters of photodetection for Au/ZnO/p-Si heterostructure in the case of 46 mM solution molarity depending on irradiance levels (A) rectification ratio, (B) photosensitivity, (C) responsivity, and (D) specific detectivity.

the degree of how much a diode blocks current at reverse bias and transmits current at forward bias.[59] The value of *RR* may decrease with increasing irradiance levels if a photodetector is highly light-sensitive. Irradiance level-dependent *RR* profile of the Au/ZnO/p-Si heterostructures both 46 and 56 mM ZnO solution molarities have been presented in Figures 7A and 8A, respectively. The *RR* value of the dark condition has been computed to be 9.166×10^2 for 46 mM solution molarity and 1.890×10^4 for 56 mM solution molarity. The *RR* values of the light illuminations decreased to lower levels at ±2 V for both devices. The reason for this decrease can attributed to increasing current at reverse biases due to photodetection behaviors of the devices as shown in *I–V* characteristics. Zeng et al. fabricated $MoTe_2$/Ta:β-Ga_2O_3 *p*-n junction with very high rectification ratio and very high responsivity by changing irrdiance level.[60]

Detection characteristics can be evaluated using photosensitivity (*K*), responsivity (*R*), specific detectivity (*D**), and external quantum efficiency (EQE) values, and they are listed by the following expressions[61]:

$$K = \frac{I_p}{I_{dark}} \tag{1}$$

$$R = \frac{I_p}{PA} \tag{2}$$

$$D^* = R\sqrt{\frac{A}{2qI_{dark}}} \tag{3}$$

$$\mathrm{EQE} = \frac{hc}{q\lambda} R\,\% \tag{4}$$

where I_p shows photocurrent and refers to the difference of the light and dark currents. The *A*, q, and *P* are detector effective area, charge of the electron, and irradiance levels, respectively. The c refers to the speed of light, h is the Planck constant, and λ is the wavelength of the incident light. Irradiance level-dependent profiles of the

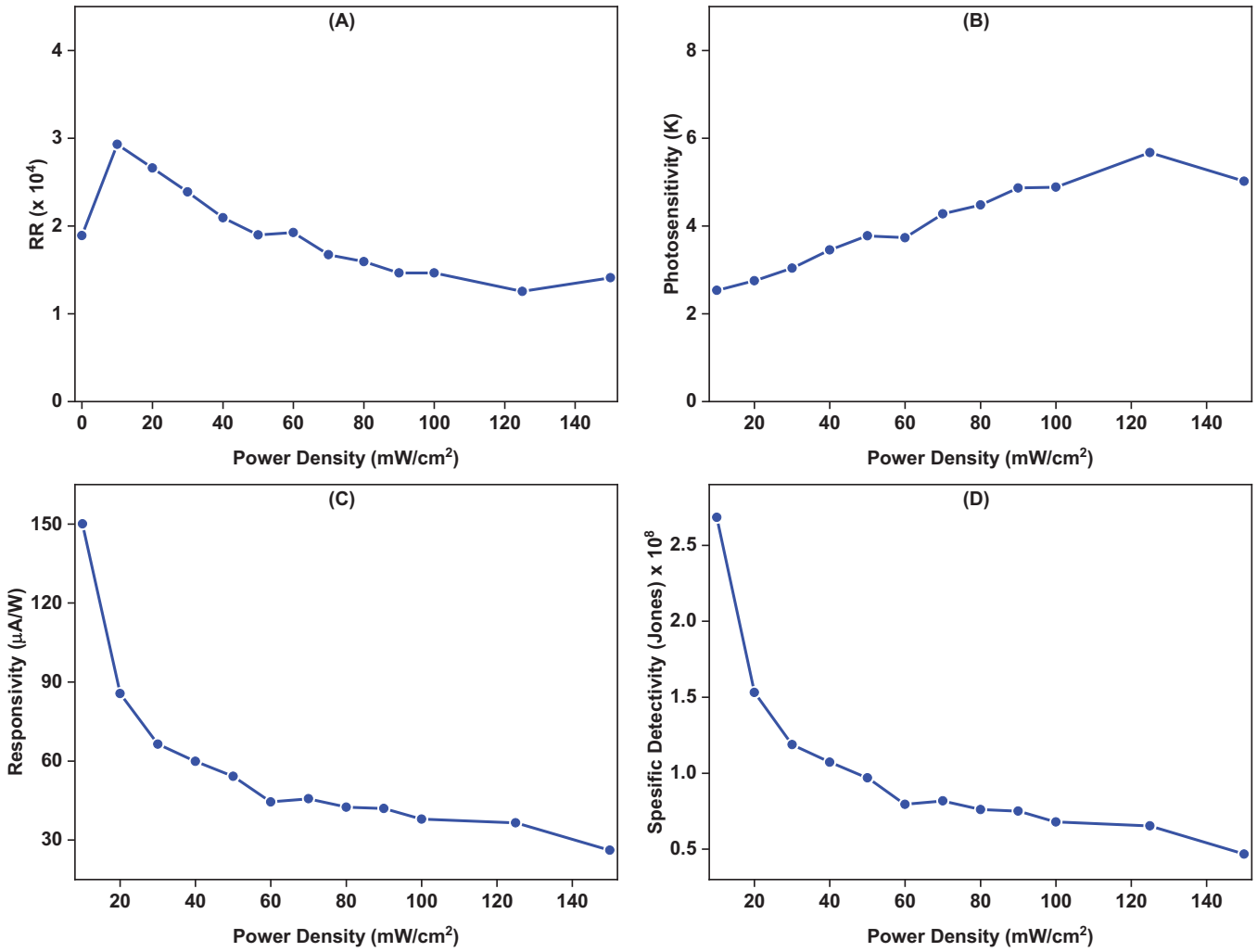

FIGURE 8 Parameters of photodetection for Au/ZnO/p-Si heterostructure in the case of 56 mM solution molarity depending on irradiance levels (A) rectification ratio, (B) photosensitivity, (C) responsivity, and (D) specific detectivity.

photosensitivity, responsivity, and specific detectivity are displayed in Figure 7B–D, respectively, for Au/ZnO/p-Si heterostructures with 46 mM ZnO solution molarity and Figure 8B–D for 56 mM ZnO solution molarity. Although the values of K increased linearly, the R and D^* values exponentially decreased and reached constant values for higher irradiance levels for both devices. The linear increase of the K values with an increment of irradiance levels and low slope highlight that the Au/ZnO/p-Si photodetectors have a photoconduction mechanism, but the trap levels cause low photosensitivity.[62] The exponential decrease at the R and D^* values may be ascribed to the complex charge transport mechanism that occurs by charge trapping and recombination. Thus, this condition causes saturation for high-level irradiance levels.[63] Furthermore, the values of I_p, K, R, and D^* have been listed in Tables 1 and 2 for changing irradiance levels in the case of 46 and 56 mM ZnO solution molarities. Although the highest K and I_p values were obtained to be 5.601 and 12.750 μA for 150 mW/cm^2 irradiance level for 46 mM ZnO solution molarity, the highest R and D^* values were determined as 92.501 mA/W and 8.705×10^9 Jones for 10 mW/cm^2 irradiance level, respectively. In the case of 56 mM solution molarity, the highest K and I_p values were obtained as 5.017 and 30.818 nA for 150 mW/cm^2 irradiance level, and the highest values of R and D^* were determined to be 150.028 μA/W and 2.684×10^8 Jones for 10 mW/cm^2 irradiance level, respectively. The photodetector with 46 mM ZnO solution molarity has better performance according to calculated detector parameters.

Figure 9A,C indicate voltage and irradiance levels-dependent profiles of responsivity for 46 and 56 mM solution molarities, respectively. When the reverse voltage increased, the responsivity values increased. However, the increase in irradiance levels induced to decrease in the responsivity values owing to the charge trapping and recombination mechanism. In addition, The Au/ZnO/p-Si heterostructures were investigated by I–V analysis for 365,

TABLE 1 Performance parameters of the Au/ZnO/p-Si heterostructure with 46 mM ZnO solution molarity for varying irradiance levels and wavelengths.

Conditions	Variations	Responsivity (mA/W)	Photosensitivity (–)	Photocurrent (A)	Specific detectivity (Jones)	EQE (%)
Power (mW/cm^2)	10	92.501	3.622	7.265×10^{-6}	8.705×10^{9}	–
	20	52.428	3.972	8.235×10^{-6}	4.934×10^{9}	–
	30	35.169	3.990	8.286×10^{-6}	3.310×10^{9}	–
	40	28.768	4.261	9.038×10^{-6}	2.707×10^{9}	–
	50	23.647	4.351	9.29×10^{-6}	2.225×10^{9}	–
	60	19.986	4.399	9.418×10^{-6}	1.881×10^{9}	–
	70	17.867	4.545	9.823×10^{-6}	1.681×10^{9}	–
	80	15.733	4.567	9.885×10^{-6}	1.481×10^{9}	–
	90	14.550	4.711	1.028×10^{-5}	1.369×10^{9}	–
	100	13.379	4.792	1.051×10^{-5}	1.259×10^{9}	–
	125	11.229	4.978	1.102×10^{-5}	1.057×10^{9}	–
	150	10.822	5.601	1.275×10^{-5}	1.018×10^{9}	–
Wavelength (nm)	365	118.639	4.362	9.318×10^{-6}	1.117×10^{10}	40.305
	395	133.775	4.791	1.051×10^{-5}	1.259×10^{10}	41.995
	850	134.423	4.810	1.056×10^{-5}	1.265×10^{10}	19.610

Abbreviation: EQE, external quantum efficiency.

TABLE 2 Performance parameters of the Au/ZnO/p-Si heterostructure with 56 mM ZnO solution molarity for varying irradiance levels and wavelengths.

Conditions	Variations	Responsivity (μA/W)	Photosensitivity (–)	Photocurrent (A)	Specific detectivity (Jones)	EQE (%)
Power (mW/cm^2)	10	150.028	2.536	1.178×10^{-8}	2.684×10^{8}	–
	20	85.620	2.753	1.345×10^{-8}	1.531×10^{8}	–
	30	66.402	3.040	1.565×10^{-8}	1.188×10^{8}	–
	40	59.925	3.454	1.883×10^{-8}	1.072×10^{8}	–
	50	54.211	3.775	2.129×10^{-8}	9.697×10^{7}	–
	60	44.453	3.731	2.095×10^{-8}	7.951×10^{7}	–
	70	45.712	4.276	2.513×10^{-8}	8.177×10^{7}	–
	80	42.512	4.482	2.671×10^{-8}	7.604×10^{7}	–
	90	41.953	4.866	2.966×10^{-8}	7.504×10^{7}	–
	100	37.938	4.884	2.980×10^{-8}	6.786×10^{7}	–
	125	36.521	5.674	3.585×10^{-8}	6.533×10^{7}	–
	150	26.159	5.017	3.082×10^{-8}	4.679×10^{7}	–
Wavelength (nm)	365	12.736	1.130	1.000×10^{-9}	2.278×10^{7}	4.327×10^{-3}
	395	0.701jjçh4	1.007	5.506×10^{-11}	1.254×10^{6}	0.220×10^{-3}
	850	13.235	1.136	1.040×10^{-9}	2.367×10^{7}	1.931×10^{-3}

Abbreviation: EQE, external quantum efficiency.

395, and 850 nm wavelengths illumination situation at 10 mW/cm^2 irradiance levels. Figure 9B,D displays the *I–V* curve of the Au/ZnO/p-Si heterostructures for dark, sun (10 mW/cm^2), and various wavelength illumination conditions in the case of 46 and 56 mM solution molarity conditions, respectively. The current increase due to increasing irradiance level for 10 mW/cm^2 at reverse biases can be seen easily. The inset of Figure 9B shows the current changes depending on the wavelength variations. According to the results, the Au/ZnO/p-Si heterostructure exhibited the highest photocurrent in the case of 850 nm illumination condition for 46 mM ZnO solution molarity. Normally, it is expected that ZnO interlayer can contribute photocurrent at the UV region due to the

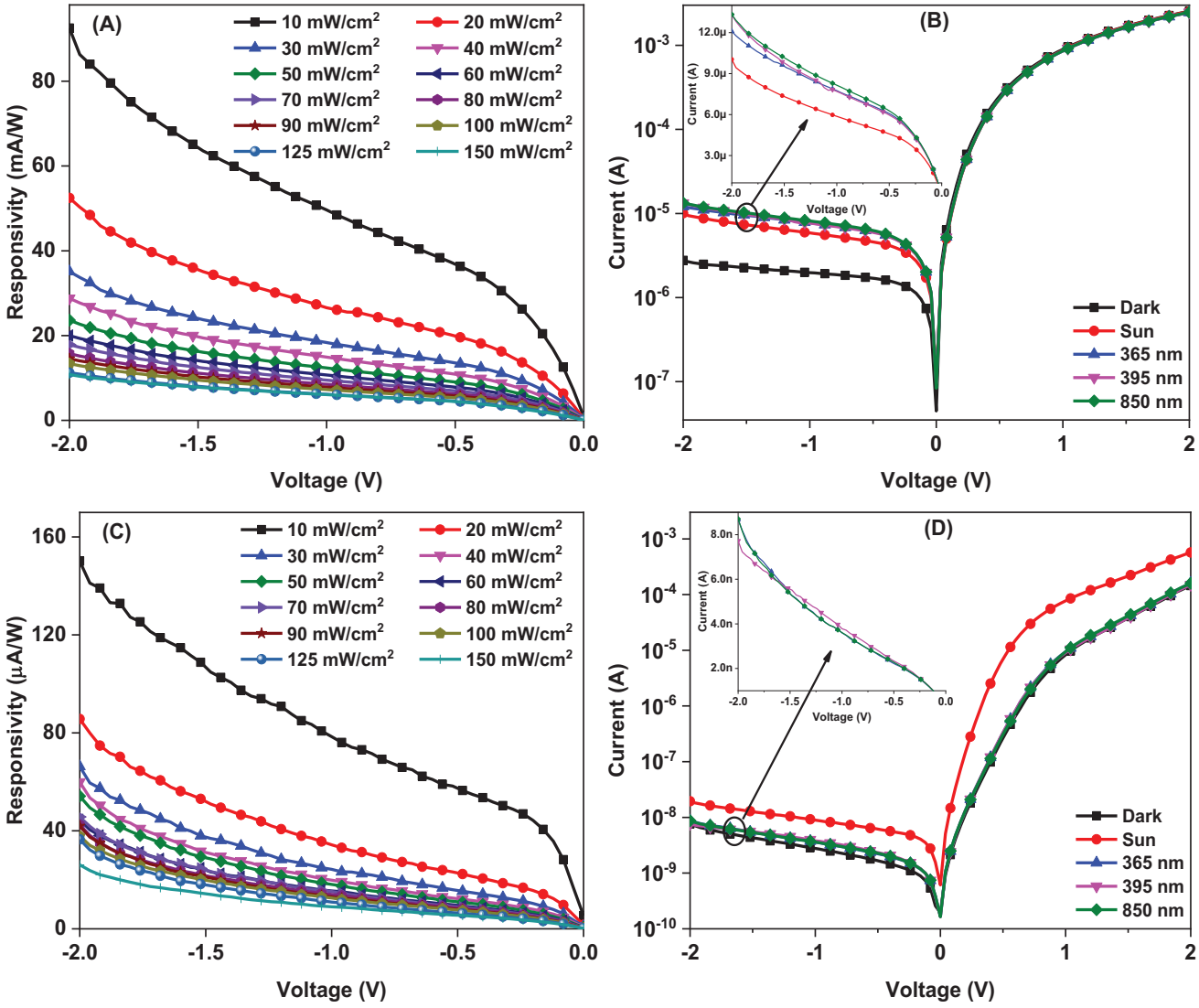

FIGURE 9 Parts (A) and (C) *R–V* plots for varying irradiance levels, and (B) and (D) *I–V* curve of the Au/ZnO/p-Si heterostructures in case of illumination wavelengths for or 46 and 56 mM ZnO solution molarities, respectively.

UV absorbance of ZnO.[64] However, the traps or defects states in the ZnO structure caused to recombination of the charges. In the case of 56 mM ZnO solution molarity condition, photocurrent did not increase more than sun condition. This can be attributed to that the interfacial states or trap levels are effective in these specific wavelengths.

The photodetection parameters were studied depending on the voltage for various wavelength values. Figure 10A–D present voltage-dependent detection parameters of the Au/ZnO/p-Si heterostructure with 46 mM ZnO solution molarity for varying wavelength values. Although Figure 10A,B shows photosensitivity and EQE profiles, Figure 10C,D displays responsivity and detectivity, respectively. The detection performance of the Au/ZnO/p-Si heterostructure with 46 mM ZnO solution molarity generally increased by increasing reverse bias. Its performance also generally increased in the case of photosensitivity, responsivity, and detectivity by increasing wavelength. However, the highest EQE value was obtained for 365 nm wavelength. Table 1 lists the photodetection parameters of the Au/ZnO/p-Si heterostructure with 46 mM solution molarity for varying wavelengths for −2 V. This Au/ZnO/p-Si heterostructure exhibited the highest photosensitivity, responsivity, and detectivity of 4.810, 134.423 mA/W, and 1.265×10^{10} Jones, respectively, for illumination at 850 nm. The highest EQE value was obtained as 40.305% at 365 nm. The reason for the high performance at 850 nm instead of 365 nm or UV region can be attributed to ZnO interlayer having many recombination centers to trap charge carriers.

Voltage-dependent detection parameters of the Au/ZnO/p-Si heterostructure with 56 mM ZnO solution molarity for varying wavelength values have been

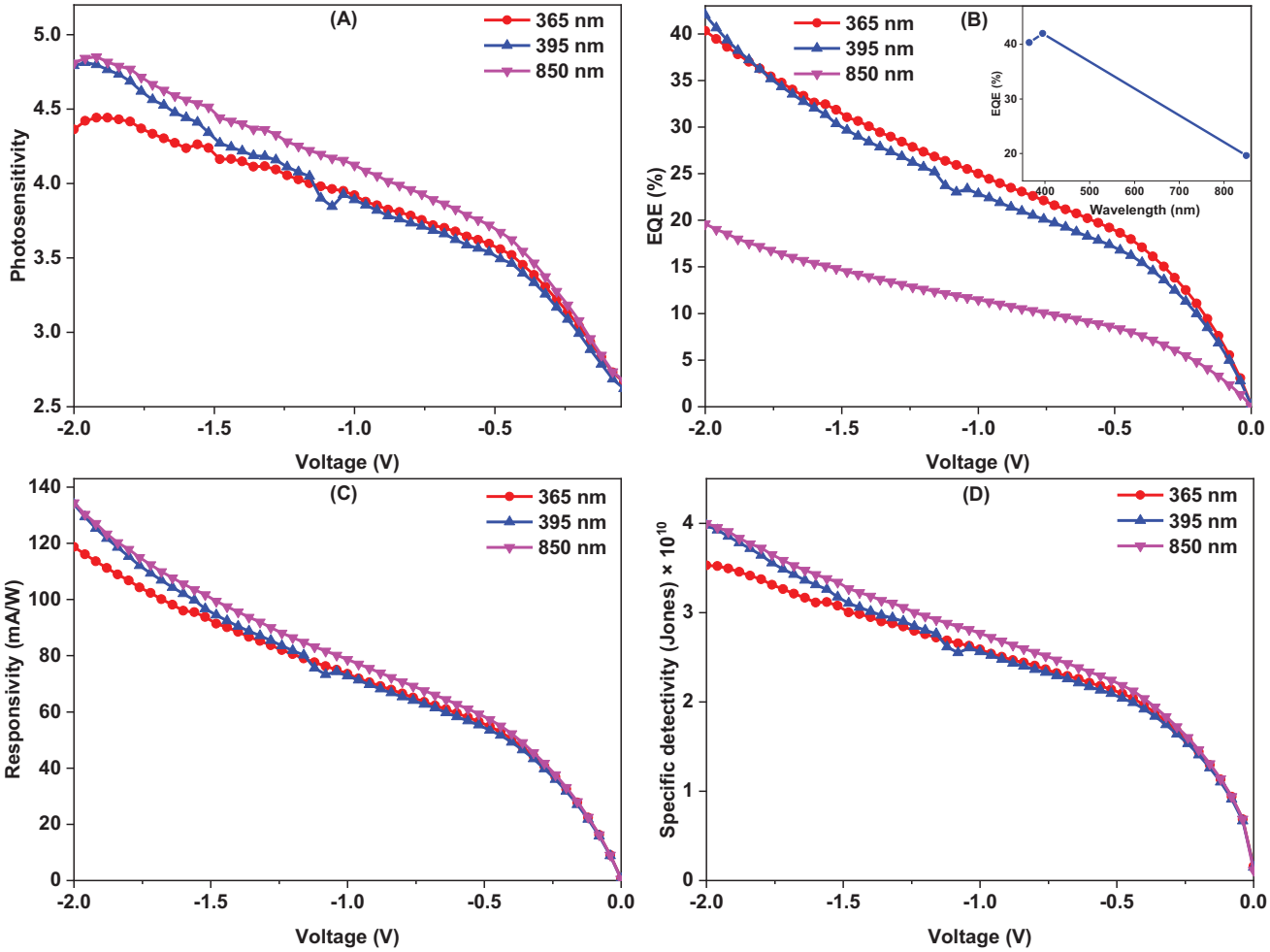

FIGURE 10 Voltage-dependent detection parameters of Au/ZnO/p-Si heterostructure with 46 mM ZnO solution molarity for varying wavelength. (A) Photosensitivity (B) external quantum efficiency (EQE) (%), (C) responsivity, and (D) specific detectivity.

shown in Figure 11A–D. Figure 11A,B exhibits photosensitivity and EQE profiles, whereas Figure 11C,D presents responsivity and detectivity, respectively. Although the photodetection performance parameters, that is, EQE, responsivity, and specific detectivity values, increased first for increasing reverse voltage and then decreased toward −2 V for almost every illuminated wavelength, the photosensitivity values generally decreased. This can be attributed to that the recombination of the charges is faster toward higher reverse voltages. Furthermore, the values of performance for the Au/ZnO/p-Si heterostructure with 56 mM ZnO solution molarity did not change much with changing wavelengths. Table 2 tabulates the detection parameters of the Au/ZnO/p-Si heterostructure with 56 mM solution molarity for varying wavelengths for −2 V. The highest EQE value was obtained for 365 nm wavelength to be 4.327×10^{-3}, whereas the highest photosensitivity, responsivity, and detectivity values were accounted as 1.136, 13.235 μA/W, and 2.367×10^{8} Jones, respectively, for illumination at 850 nm. The low performance of the ZnO interlayer with 56 mM solution molarity can be ascribed to the conductivity performance of the ZnO or trap levels. In that way, Li et al. confirmed that the suppressing of the defects can decrease effectively non-radiative recombination to improve the performance of a photodetector.[65]

We also compared our results with those of previous studies in the literature. Table 3 displays the performance of the last ZnO-based photodetector results compared with this study. According to Table 3, the obtained performance of the photodetectors is in good agreement with the current literature. The fabrication atmosphere, methods, device structures, and used materials are not the same as these heterostructures, and we cannot completely compare our results with previous studies. However, the comparison can give some information about performances of the fabricated devices.

The impedance spectroscopy analysis has been employed to determine the effects of interfacial trap states of Au/ZnO/p-Si heterostructure in case of changing

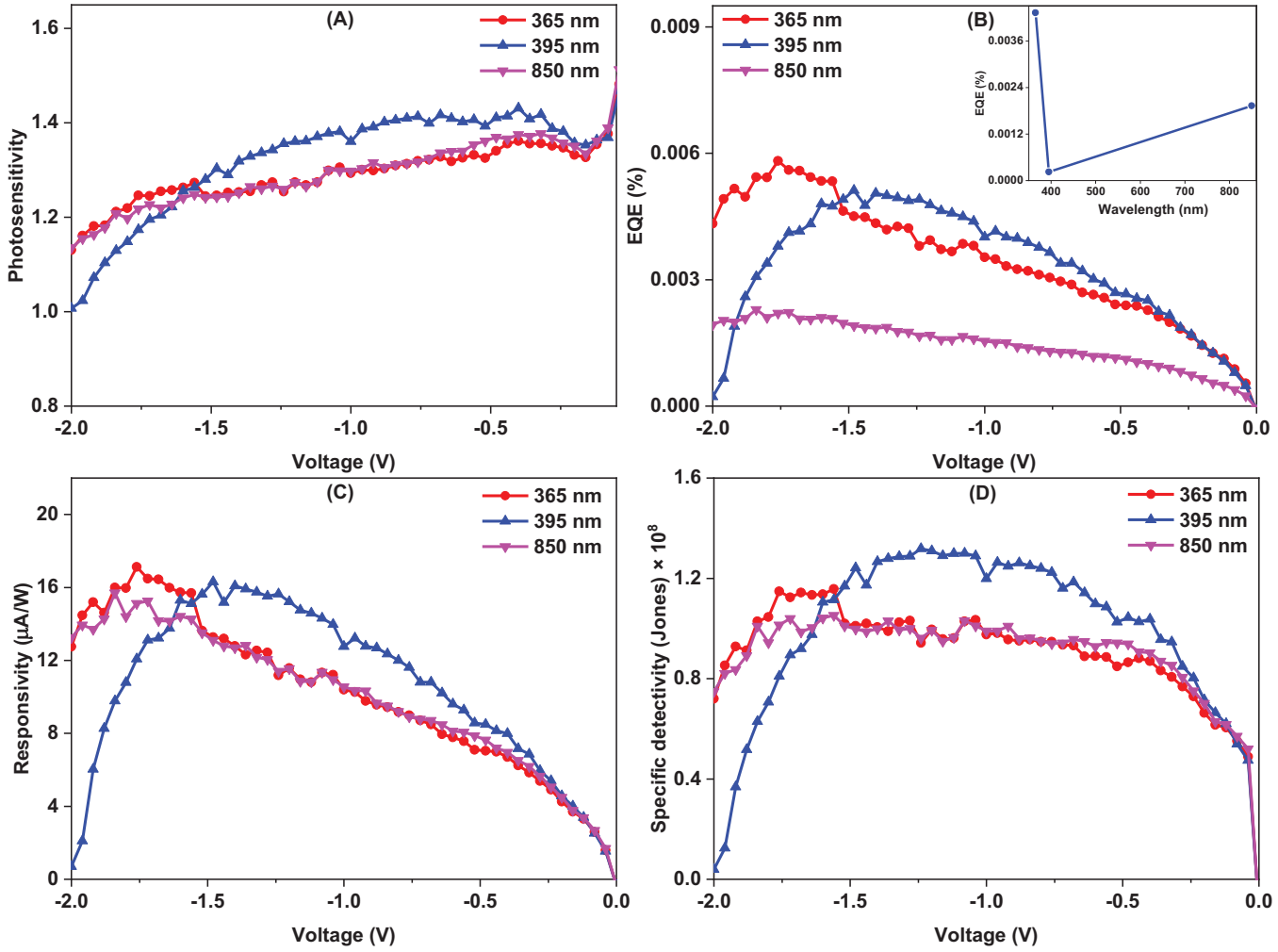

FIGURE 11 Voltage-dependent detection parameters of Au/ZnO/p-Si heterostructure with 46 mM ZnO solution molarity for varying wavelength. (A) Photosensitivity (B) external quantum efficiency (EQE) (%), (C) responsivity, and (D) specific detectivity.

frequencies because capacitance and conductance investigations are useful. The filling of trap states in the band gap can induce a variation in the capacitance values of the heterostructure due to electrons that can fill the lower conduction band or be emitted to the valance band. Thus, frequency-dependent *C–V* characteristics can help to determine the condition of the trap state levels.[73] Figure 12A,C introduces *C–V*, and Figure 12B,D displays *G–V* curves of the Au/ZnO/p-Si heterostructures with 46 and 56 mM ZnO solution molarities, respectively, for varying frequencies from 10 kHz to 1 MHz. Both conductance and capacitance values are changed by voltage. However, the conductance values stayed constant, whereas the capacitance values reduced as the frequency increased. The failure of the interface states to chase the AC signal is responsible for the decrease in capacitance values with increments of frequency.[74] Generally, the detected capacitance of Schottky heterostructure changes by frequency and voltage due to impurity level, Schottky barrier feature, interface states, series resistance, or interfacial layer between semiconductor and metal. Although usually interface states are effective at lower frequencies on capacitance, series resistance is effective at higher frequencies.[75] The interface states and resistance of the Au/ZnO/p-Si heterostructures are calculated using impedance spectroscopy analysis to investigate the effect on the devices. The *C–V* and *G–V* curves and C^{-2}–*V* graphs can be used to compute these parameters. The results obtained are in agreement with the previous literature on ZnO-based interlayers.[29,76–78]

The Nicollian and Brews technique is generally utilized to calculate the resistance (R_i) of the Au/ZnO/p-Si heterostructure with varying frequency using the following equation:

$$R_i = \frac{G_m}{G_m^2 + (\omega C_m)^2} \tag{5}$$

TABLE 3 The comparisons of Au/ZnO/p-Si photodetectors some of the previous results.

Structure	I_p (A)	K (—)	R (mA/W)	D^* (Jones)	EQE (%)	Wavelength (nm)	Refs.
GR/ZnO NW/GR	6.05×10^{-6}	800	420.0	–	–	325	66
Au/ZnO/p-Si	6.09×10^{-6}	7.93	77.51	1.30×10^{10}	26.33	365	46
ZnO:GQD	–	–	500	2.11×10^{11}	–	365	67
Au/In:ZnO/Au	–	71.4	2500	1.44×10^{11}	–	390	68
Au/ZnO/p-Si	–	–	441.2	39.2×10^{12}	–	360	69
Pd/CdO/ZnO	–	–	12 900	2.90×10^{9}	–	375	70
Au/ZnO/p-Si	1.22×10^{-6}	–	380	–	–	360	71
Ag/ZnO/Al	30.0×10^{-6}	–	200	7.66×10^{10}	–	Sun	72
Au/ZnO/p-Si	10.51×10^{-6}	4.79	133.77	1.26×10^{10}	41.99	395	This work

Abbreviation: EQE, external quantum efficiency; GR, shows graphene; NW, indicates nanowire.

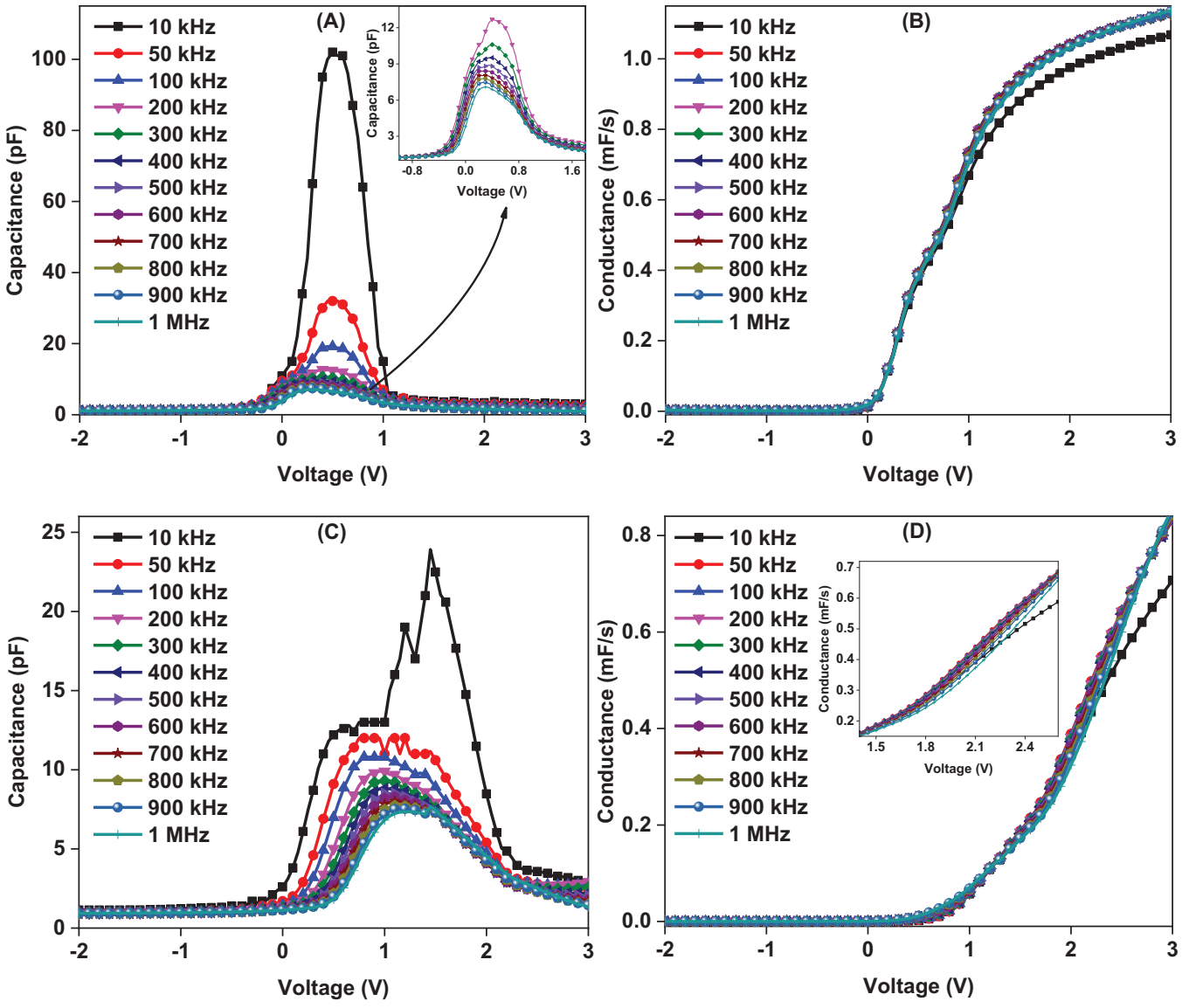

FIGURE 12 Parts (A) and (C) exhibit *C–V*, (B) and (D) display *G–V* characteristics of the Au/ZnO/p-Si heterostructure with 46 and 56 mM ZnO solution molarities for various frequencies, respectively.

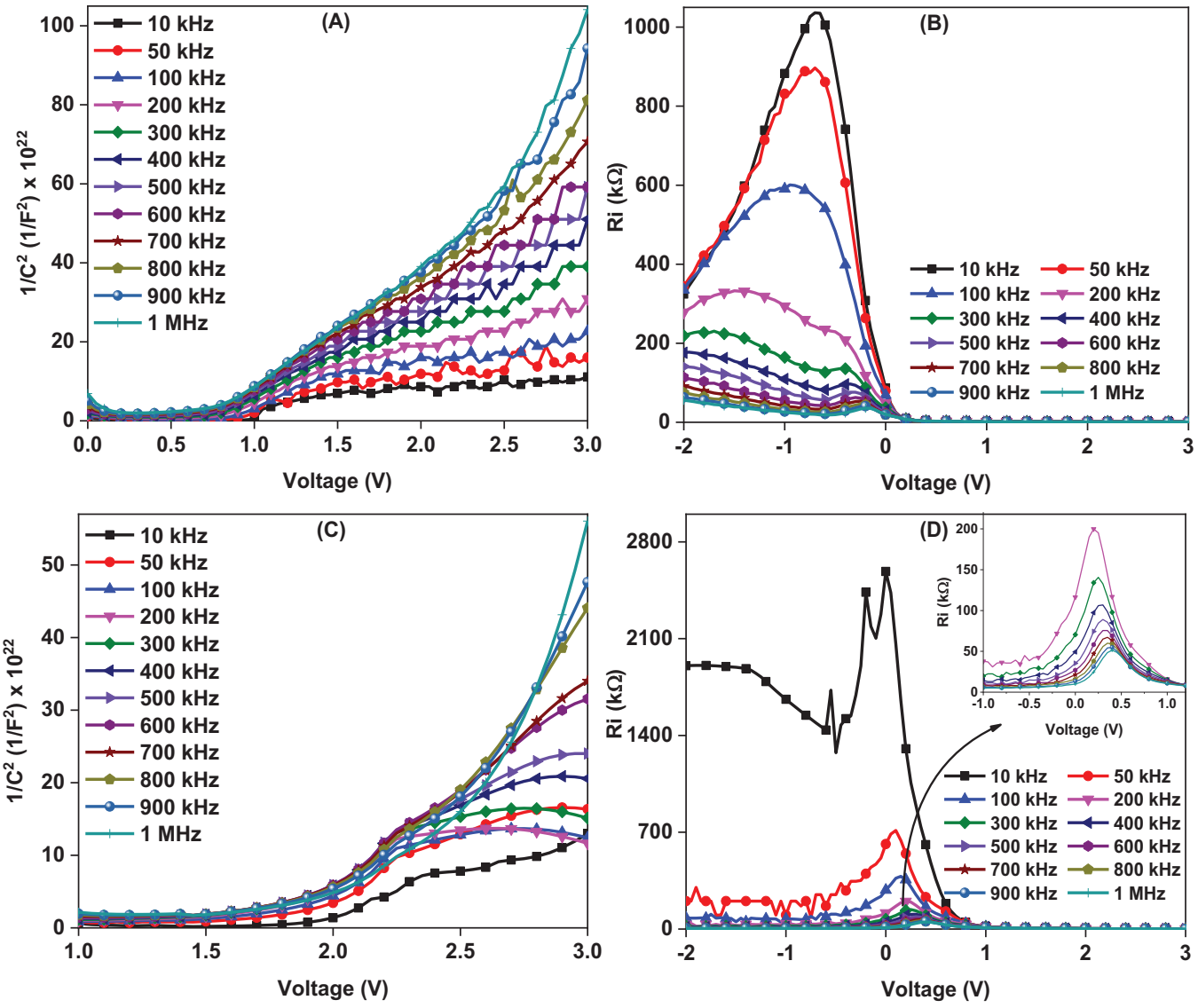

FIGURE 13 Parts (A) and (C) exhibit C^{-2}–V *plots* and (B) and (D) show R_i–V graphs of the Au/ZnO/p-Si heterostructure with 46 and 56 mM ZnO solution molarities for various frequencies, respectively.

where ω indicates the angular frequency, G_m and C_m are the detected conductance and capacitance subsequently. From the slope and x-intercept of the C^{-2}–V plots, several electrical variables are calculated, that is, the width of the depletion region (W_d), the maximum electric field (E_m), the Fermi energy levels (E_F), the carrier concentration of the acceptor atoms (N_a), and the barrier height. The equations for calculating those values based on the C^{-2}–V diagrams are available everywhere.[79] Among these, Φ_b is defined by the following equation[80]:

$$\Phi_b = (V_d + E_F) - \Delta\Phi \tag{5}$$

where $\Delta\Phi$ is barrier lowering of image force and V_d is the diffusion potential obtained by the equation of $V_d = V_i + kT/q$, separately. Here, V_i is the x-intercept extrapolated from the voltage axis for C^{-2}–V plots.

Figure 13A,C shows the C^{-2}–V plots of the Au/ZnO/p-Si heterostructures for 46 and 56 mM ZnO solution molarities, whereas Figure 13B,D presents R_i–V curves of the Au/ZnO/p-Si heterostructures for different frequencies from 100 kHz to 1 MHz. Both the C^{-2}–V plots and R_i–V curves of the Au/ZnO/p-Si heterostructures changed with changing frequency and voltage. R_i–V graphs revealed a decreasing profile and exhibited peaks, and the peak positions changed with increasing frequency. These behaviors can be attributed to the distribution of the interface states and their restructuring and reordering by applying the electric field.[81,82] Furthermore, the Au/ZnO/p-Si heterostructure with 46 mM solution molarity has a different R_i–V profile than with 56 mM solution molarity

TABLE 4 The calculated electrical parameters of the Au/ZnO/p-Si heterostructure with 46 mM ZnO solution molarity for varying frequency.

F (kHz)	N_a (10^{12} cm^{-3})	Φ_b (eV)	E_F (eV)	E_m (10^3 V/cm)	W_d (10^{-4} cm)	ε
10	4.163	0.472	0.339	0.371	6.531	9.409
50	2.981	0.538	0.348	0.388	9.205	8.201
100	2.492	0.560	0.353	0.373	10.529	7.510
200	1.746	0.676	0.362	0.392	15.432	6.733
300	1.271	0.876	0.370	0.431	22.936	6.215
400	1.040	0.968	0.375	0.424	27.440	5.697
500	0.904	1.030	0.379	0.415	30.831	5.266
600	0.822	1.047	0.381	0.401	32.699	4.920
700	0.747	1.070	0.384	0.388	34.812	4.532
800	0.688	1.093	0.386	0.378	36.837	4.204
900	0.645	1.114	0.388	0.371	38.562	3.824
1000	0.619	1.143	0.389	0.370	40.097	3.289

TABLE 5 The calculated electrical parameters of the Au/ZnO/p-Si heterostructure with 56 mM ZnO solution molarity for varying frequency.

F (kHz)	N_a (10^{13} cm^{-3})	Φ_b (eV)	E_F (eV)	E_m (10^3 V/cm)	W_d (10^{-4} cm)	ε
10	5.605	0.944	0.272	3.332	3.990	9.351
50	1.367	1.092	0.309	1.779	8.712	6.114
100	0.908	1.174	0.319	1.516	11.159	5.287
200	0.706	1.203	0.326	1.354	12.815	4.927
300	0.616	1.242	0.329	1.292	13.997	4.640
400	0.557	1.271	0.332	1.246	14.925	4.496
500	0.500	1.309	0.335	1.203	16.041	4.388
600	0.455	1.346	0.337	1.168	17.121	4.316
700	0.437	1.378	0.338	1.163	17.735	4.226
800	0.412	1.405	0.340	1.143	18.476	4.165
900	0.393	1.428	0.341	1.129	19.098	4.093
1000	0.370	1.473	0.342	1.116	20.079	4.053

due to having various amounts of interface states. These can be attributed to heterostructures having different frequency-dependent charges, that is, mobile oxide, fixed, or interfacial charges.[83] Tables 4 and 5 show the electrical parameter values of the Au/ZnO/p-Si heterostructures with 46 and 56 mM ZnO solution molarities for various frequencies calculated from C^{-2}–V plots, respectively. Although the value of N_a decreases, the Φ_b, E_F, and W_d parameters increase as the frequency increases for both heterostructures. However, the E_m values of Au/ZnO/p-Si heterostructures with 46 mM solution molarity increased toward 500 kHz and then decreased again up to 1 MHz. The E_m values of Au/ZnO/p-Si heterostructures with the 56 mM solution molarity decreased by increasing frequency. Most of the calculated parameters are almost the same level for the Au/ZnO/p-Si heterostructures with 46 and 56 mM ZnO solution molarities. The results of N_a are lower than the literature due to low level capacitance values.[84]

The real part dielectric constant (ε) of the Au/ZnO/p-Si heterostructure with 46 and 56 mM ZnO solution molarities was calculated by the formalism of $\varepsilon = C_m/C_0$ where C_0 shows free-space capacitor value and given in Tables 4 and 5 for various capacitance values at 0 voltage. The results revealed that the Au/ZnO/p-Si heterostructure has a dielectric constant of around 9 at 10 kHz, and their values decreased slightly by increasing frequency. These results are in good agreement with the literature.[29,85,86] Furthermore, the increasing molarity of the ZnO from 46 to 56 mM caused the converging of dielectric constant values around 4 after 100 kHz frequency. This converging at the ε values of the Au/ZnO/p-Si heterostructure with 56 mM solution molarity can be attributed to the freezing or not responding of the interface states toward higher frequency.[86]

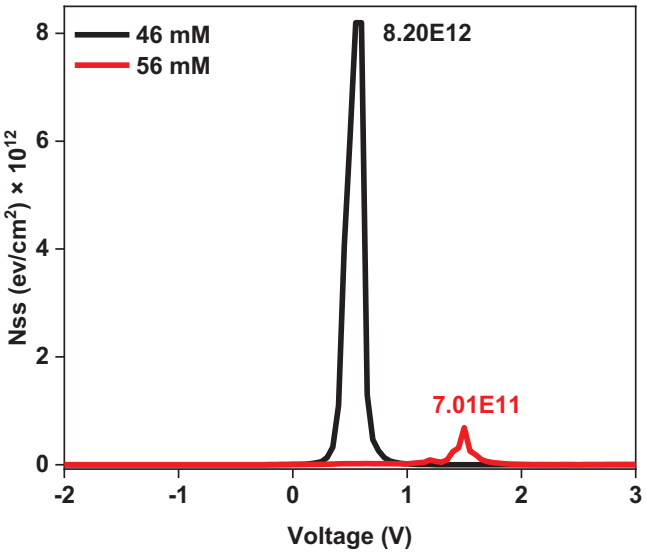

FIGURE 14 Voltage-dependent N_{ss} profiles for Au/ZnO/p-Si heterostructures with 46 and 56 mM ZnO solution molarities.

Furthermore, the calculation of the interface states density (N_{ss}) can be obtained by following the formula with low-high frequency capacitance (C_{LF}–C_{HF}) technique[82]:

$$N_{ss} = \frac{1}{qA}\left[\left(\frac{1}{C_{LF}} - \frac{1}{C_i}\right)^{-1} - \left(\frac{1}{C_{HF}} - \frac{1}{C_{0x}}\right)^{-1}\right] \quad (6)$$

where C_{LF} and C_{HF} are low and high frequency capacitance, and C_{0x} is interfacial layer capacitance which obtained by next equation depending on the capacitance (C_m) and conductance (G_m) parameters. The C_{0x} is calculated for the zone of strong accumulation with formula of:

$$C_{0x} = C_{ma}\left[1 + \frac{G_{ma}^2}{(\omega C_{ma})^2}\right] \quad (7)$$

where G_{ma} and C_{ma} are the measured maximum conductance and capacitance values, respectively. Figure 14 shows voltage-dependent N_{ss} profiles for Au/ZnO/p-Si heterostructures with 46 and 56 mM ZnO solution molarities. According to this graph, the N_{ss} values are almost 10-fold higher for the heterostructure of Au/ZnO/p-Si with 46 and 56 mM ZnO solution molarities due to maybe its ZnO interfacial morphological structure as shown in Figure 1. Furthermore, the changing molarity of the ZnO solution caused to change the region and intensity of the peaks due to increasing passivation amount of the ZnO. Such peak properties and changing peak position by increasing solution molarity can be attributed to the partial distribution of the N_{ss} in the bandgap of Si or restructuring or reordering of charges and traps.[87]

4 | CONCLUSION

ZnO structures were easily synthesized on p-Si by a hydrothermal route for different molarity concentrations of 46 and 56 mM, and they were investigated by SEM and XRD techniques for structural characterization. The SEM results confirmed the flower-like structures with changing molarity, whereas the XRD pattern indicated the hexagonal wurtzite phase of the ZnO. The ZnO structures were employed to construct the Au/ZnO/p-Si heterostructures to investigate their photodetection capability as an interfacial layer between the Au and p-Si substrates. The *I–V* analyses were performed for Au/ZnO/p-Si heterostructure at a range of irradiance levels (dark to 150 mW/cm^2) and wavelength values of 365, 395, and 850 nm. The impedance spectroscopy technique was also employed to determine interface states on the Au/ZnO/p-Si heterostructures. The ideality factor, series resistance, and barrier height values were determined to be 2.152, 1.012 kΩ and 0.612 eV for the Au/ZnO/p-Si heterostructure with 46 mM solution molarity and 2.085, 3.349 MΩ, and 0.826 eV for the Au/ZnO/p-Si heterostructure with 56 mM solution molarity, respectively. Although photosensitivity values increased linearly by increasing irradiance levels, specific detectivity and responsivity values exponentially decreased for both Au/ZnO/p-Si heterostructures. The highest responsivity and specific detectivity values were obtained to be 134.423 mA/W and 1.265 × 10^{10} Jones, respectively, for illumination at 850 nm for the Au/ZnO/p-Si heterostructure with 46 mM solution molarity. The maximum EQE value was obtained again with Au/ZnO/p-Si heterostructure with 46 mM solution molarity as 40.305% at 365 nm. The *C–V* characteristics confirmed the frequency and voltage-dependent profiles of the Au/ZnO/p-Si heterostructures.

ACKNOWLEDGMENTS

The authors would like to thanks Fatma Yildirim and Çiğdem Eden.

ORCID

Mustafa Coşkun https://orcid.org/0000-0002-9716-4444
Adem Kocyigit https://orcid.org/0000-0002-8502-2860

REFERENCES

1. Danish MSS, Bhattacharya A, Stepanova D, Mikhaylov A, Grilli ML, Khosravy M, et al. A systematic review of metal oxide applications for energy and environmental sustainability. Metals (Basel). 2020;10:1604.
2. Yilmaz M., Aydoğan Ş. The effect of Mn incorporation on the structural, morphological, optical, and electrical features of nanocrystalline ZnO thin films prepared by chemical spray pyrolysis technique. Metall Mater Trans A. 2015;46(6):2726–35. https://doi.org/10.1007/s11661-015-2875-7

3. Grilli ML, Valerini D, Rizzo A, Yilmaz M, Song C, Hu G, et al. A comparative study of the mechanical and tribological properties of thin Al_2O_3 coatings fabricated by atomic layer deposition and radio frequency sputtering. Phys Status Solidi (a). 2021;219(1):Portico. https://doi.org/10.1002/pssa.202100398
4. Orak I, Kocyigit A, Turut A. The surface morphology properties and respond illumination impact of ZnO/n-Si photodiode by prepared atomic layer deposition technique, J. Alloys Compd. 2017;691:873–79.
5. Sharma DK, Shukla S, Sharma KK, Kumar V. A review on ZnO: Fundamental properties and applications, Mater. Today Proc. 2022;49:3028–35.
6. Chen Y, Su L, Jiang M, Fang X. Switch type PANI/ZnO core-shell microwire heterojunction for UV photodetection, J. Mater. Sci. Technol. 2022;105:259–65.
7. Zhang Z, Ning Y, Fang X. From nanofibers to ordered ZnO/NiO heterojunction arrays for self-powered and transparent UV photodetectors. J. Mater. Chem. C. 2019;7:223–29.
8. Yilmaz M, Aydoğan Ş. The effect of Pb doping on the characteristic properties of spin coated ZnO thin films: Wrinkle structures. Mater Sci Semicond Process. 2015;40:162–70. https://doi.org/10.1016/j.mssp.2015.06.064
9. Özmen A, Aydogan S, Yilmaz M. Fabrication of spray derived nanostructured n-ZnO/p-Si heterojunction diode and investigation of its response to dark and light. Ceram Int. 2019;45:14794–805. https://doi.org/10.1016/j.ceramint.2019.04.210
10. Kolodziejczak-Radzimska A, Jesionowski T. Zinc oxide-from synthesis to application: a review. Materials (Basel). 2014;7:2833–81.
11. Kocyigit A, Orak I, Çaldıran Z, Turut A. Current–voltage characteristics of Au/ZnO/n-Si device in a wide range temperature. J. Mater. Sci. Mater. Electron. 2017;28:17177–84.
12. Doyan A, Fitri SA, Ahzan S. Crystal structure characterization of thin layer zinc oxide. IOP Conference Series: Materials Science and Engineering. 2017;196:12004.
13. Rajasekaran M, Arunachalam A, Kumaresan P. Structural, morphological and optical characterization of Ti-doped ZnO nanorod thin film synthesized by spray pyrolysis technique. Mater. Res. Express. 2020;7:036412.
14. Adeleye AT, John KI, Adeleye PG, Akande AA, Banjoko OO. One-dimensional titanate nanotube materials: heterogeneous solid catalysts for sustainable synthesis of biofuel precursors/value-added chemicals—a review. J. Mater. Sci. 2021;56:18391–416.
15. Mohan S, Vellakkat M, Aravind A. UR hydrothermal synthesis and characterization of zinc oxide nanoparticles of various shapes under different reaction conditions. Nano Express. 2020;1:030028.
16. Dutta T, Noushin T, Tabassum S, Mishra SK. Road map of semiconductor metal-oxide-based sensors: a review. Sensors. 2023;23:6849.
17. Qiu Z, Shen X, Zhao Z. Development trends and prospects of semiconductor devices and technology. Highlights. Sci. Eng. Technol. 2024;81:374–80.
18. Oba F, Kumagai Y. Design and exploration of semiconductors from first principles: a review of recent advances. Appl. Phys. Express. 2018;11:060101.
19. Li X. Optoelectronic devices. Cambridge: Cambridge University Press; 2009.
20. Liu JM. Photodetection. In: Principles of photonics. Cambridge: Cambridge University Press; 2016. p. 362–95.
21. Chetia A, Bera J, Betal A, Sahu S. A brief review on photodetector performance based on zero dimensional and two dimensional materials and their hybrid structures Mater. Today Commun. 2022;30:103224.
22. Yan T, Yang W, Wu L, Fang X. High-work-function transparent electrode with an enhanced air-stable conductivity based on AgNiCu core-shell nanowires for Schottky photodiode. J. Mater. Sci. Technol. 2025;209:95–102.
23. Song W, Chen J, Li Z, Fang X. Self-powered MXene/GaN van der waals heterojunction ultraviolet photodiodes with superhigh efficiency and stable current outputs. Adv. Mater. 2021;33:2101059.
24. Quimby RS. Photodiode detectors. In: Photonics and lasers. Hoboken, NJ, USA: John Wiley & Sons, Inc; 2006. p. 249–79.
25. Ezhilmaran B, Patra A, Benny S, Sreelakshmi MR, Venkataprasad Bhat S., Bhat SV, et al. Recent developments in the photodetector applications of Schottky diodes based on 2D materials. J. Mater. Chem. C. 2021;9:6122–50.
26. Quimby RS. Photonics and lasers: an introduction. Hoboken: John Wiley and Sons; 2006.
27. Pathak S. Photonics integrated circuits. In: Nanoelectronics. Amsterdam: Elsevier; 2019. p. 219–70.
28. Eng PC, Song S, Ping B. State-of-the-art photodetectors for optoelectronic integration at telecommunication wavelength. Nanophotonics. 2015;4:277–302.
29. Nezhadesm-Kohardafchahi S, Farjami-Shayesteh S, Badali Y, Altındal, Jamshidi-Ghozlu MA, Azizian-Kalandaragh Y. Formation of ZnO nanopowders by the simple ultrasound-assisted method: exploring the dielectric and electric properties of the Au/(ZnO-PVA)/n-Si structure. Mater. Sci. Semicond. Process. 2018;86:173–80.
30. Akbaş AM, Çiçek O, Altındal Ş, Azizian-Kalandaragh Y. Frequency response of *C–V* and G/ω-V characteristics of Au/(Nanographite-doped PVP)/n-Si structures. J. Mater. Sci. Mater. Electron. 2020;32:993–1006.
31. Demirezen S, ÇHG, Altındal. Doping rate, interface states and polarization effects on dielectric properties, electric modulus, and AC conductivity in PCBM/NiO:ZnO/p-Si structures in wide frequency range. Silicon. 2022;1:1–11.
32. Li S, Liu X, Yang H, Zhu H, Fang X. Two-dimensional perovskite oxide as a photoactive high-κ gate dielectric. Nat. Electron. 2024;7:216–24.
33. Deka Boruah B. Zinc oxide ultraviolet photodetectors: rapid progress from conventional to self-powered photodetectors. Nanoscale Adv. 2019;1:2059–85.
34. Khaghanpour Z, Naghibi S. Perforated ZnO nanoflakes as a new feature of ZnO achieved by the hydrothermal-assisted sol–gel technique. J. Nanostructure Chem. 2017;7:55–59.
35. Orak İ, Koçyiğit A. The thickness effect of insulator layer between the semiconductor and metal contact on C–V characteristics of Al/Si3N4/p-Si device *Pamukkale Univ*. J. Eng. Sci. 2017;23:536–42.
36. Yıldız DE, Kocyigit A, Yıldırım M. Comparison of Al/TiO_2/p-Si and Al/ZnO/p-Si photodetectors. Opt. Mater. (Amst). 2023;145:114371.
37. Yilmaz M, Kocyigit A, Cirak BB, Kacus H, Incekara U, Aydogan S. The comparison of Co/hematoxylin/n-Si and

Co/hematoxylin/p-Si devices as rectifier for a wide range temperature. Mater. Sci. Semicond. Process. 2020;113:105039.
38. Jiang CY, Sun XW, Lo GQ, Kwong DL, Wang JX. Improved dye-sensitized solar cells with a ZnO-nanoflower photoanode. Appl. Phys. Lett. 2007;90: 263501.
39. Liu Y, Sun SH, Xu J, Zhao L, Sun HC, Li J, et al. Broadband antireflection and absorption enhancement by forming nano-patterned Si structures for solar cells. Opt. Express. 2011;19:A1051.
40. Das A, Mathan Kumar P, Bhagavathiachari M, Nair RG. Shape selective flower-like ZnO nanostructures prepared via structure-directing reagent free methods for efficient photocatalytic performance Mater. Sci. Eng. B. 2021;269:115149.
41. Huynh HND, Nguyen BGM, Dinh TM, Nguyen NM, Tran CK, Nguyen TT, et al. Enhancing the performance of ZnO-based photodetectors by forming ZnO/(Cu:ZnO) core/shell nanorods ACS Appl. Electron. Mater. 2024;6:1894–903.
42. Pallavolu MR, Maddaka R, Viswanath SK, Banerjee AN, Kim M-D, Joo SW. High-responsivity self-powered UV photodetector performance of pristine and V-doped ZnO nano-flowers. Opt. Laser Technol. 2023;157:108776.
43. Sharma S, Sharma Y, Sharma J. Synthesis and characterization of ZnO flower-like structures. Smart Sci. 2016;4:8–13.
44. Aydoğan Ş, Grilli ML, Yilmaz M, Çaldiran Z, Kaçuş H. A facile growth of spray based ZnO films and device performance investigation for Schottky diodes: Determination of interface state density distribution. J Alloys Compd. 2017;708:55–66.
45. Soylu M. Solution molarity dependent structural and optical properties of CdO nanostructured thin films. Optik (Stuttg). 2020;216:164865.
46. Eden C, Kocyigit A, Aydogan S, Cirak C, Yilmaz M. Detection performance of flower-like hydrothermally synthesized ZnO in silicon-type photodetector. Phys. Scr. 2024;99:065945.
47. Li Y, Xu CY, Wang JY, Zhen L. Photodiode-like behavior and excellent photoresponse of vertical Si/monolayer MoS_2 heterostructures. Sci. Rep. 2014;4:1–8.
48. Ryu S, Nguyen DC, Ha NY, Park HJ, Ahn YH, Park J-Y, et al. Light intensity-dependent variation in defect contributions to charge transport and recombination in a planar MAPbI3 perovskite solar. Cell Sci. Rep. 2019;9:19846.
49. Turut A. Thermal sensitivity from current-voltage-measurement temperature characteristics in Au/n-GaAs Schottky contacts. Turkish J. Phys. 2021;45:268–80.
50. Norde H. A modified forward I-V plot for Schottky diodes with high series resistance J. Appl. Phys. 1979;50:5052–53.
51. Cheung SK, Cheung NW. Extraction of Schottky diode parameters from forward current-voltage characteristics Appl. Phys. Lett. 1986;49:85.
52. Gumus I, Aydogan S. Thermal sensing capability of metal/composite-semiconductor framework device with the low barrier double Gaussian over wide temperature range. Sensors Actuators A Phys. 2021;332:113117.
53. Gullu HH, Yildiz DE, Toppare L, Cirpan A. Electrical characteristics of organic heterojunction with an alternating benzotriazole and fluorene containing copolymer J. Mater. Sci. Mater. Electron. 2020;31:18816–31.
54. Roul B, Mukundan S, Chandan G, Mohan L, Krupanidhi SB. Barrier height inhomogeneity in electrical transport characteristics of InGaN/GaN heterostructure interfaces. AIP Adv. Appl. Phys. Lett. 2015;5:162111–37130.
55. Barkhordari A, Ozcelik S, Altindal Ş, Pirgholi-Givi G, Mashayekhi H, Azizian-Kalandaragh Y. The effect of PVP: $BaTiO_3$ interlayer on the conduction mechanism and electrical properties at MPS structures. Phys. Scr. 2021;96:085805.
56. Kocyigit A, Yıldız DE, Hussaini AA, Kose DA, Yıldırım M. Cu and Mn centered nicotinamide/nicotinic acid complexes for interlayer of Schottky photodiode Curr. Appl. Phys. 2023;45:53–63.
57. Wang Y, Yang S, Ballesio A, Parmeggiani M, Verna A, Cocuzza M, et al. The fabrication of Schottky photodiode by monolayer graphene direct-transfer-on-silicon. J. Appl. Phys. 2020;128:014501.
58. Karataş Ş, Berk N. Performance of the illumination dependent electrical and photodiode characteristic of the Al/(GO:PTCDA)/p-Si structures. Opt. Mater. (Amst). 2022;126:112231.
59. Ferchichi K, Pecqueur S, Guerin D, Bourguiga R, Lmimouni K. High rectification ratio in polymer diode rectifier through interface engineering with self-assembled monolayer. Electron. Mater. 2021;2:445–53.
60. Zeng G, Zhang M-R, Chen Y-C, Li X-X, Chen D-B, Shi C-Y, et al. A solar-blind photodetector with ultrahigh rectification ratio and photoresponsivity based on the MoTe2/Ta:β-Ga_2O_3 pn junction. Mater. Today Phys. 2023;33:101042.
61. Gong K, Li L, Yu W, Mu H, Yuan J, Hao R, et al. High detectivity and fast response avalanche photodetector based on GaSe/PtSe2p–n junction. Mater. Des. 2023;228:111848.
62. Xu H, Wu J, Feng Q, Mao N, Wang C, Zhang J. High responsivity and gate tunable graphene-MoS_2 hybrid phototransistor. Small. 2014;10:2300–2306.
63. Chen J, Zhang Z, Feng J, Xie X, Jian A, Li Y, et al. 2D InSe self-powered schottky photodetector with the same metal in asymmetric contacts Adv. Mater. Interfaces. 2022;9:2200075.
64. Pudukudy M, Yaakob Z. Facile synthesis of quasi spherical ZnO nanoparticles with excellent photocatalytic activity. J. Clust. Sci. 2015;26:1187–201.
65. Li C, Wu Q, Liang A, Chen G, Chen S, Su Z, et al. Suppressing CuZn deep-level trap for ultrafast response in kesterite photodetector. Surfaces and Interfaces. 2024;52:104853.
66. Fu X-W, Liao Z-M, Zhou Y-B, Wu H-C, Bie Y-Q, Xu J. Graphene/ZnO nanowire/graphene vertical structure based fast-response ultraviolet photodetector. Appl. Phys. Lett. 2012;100:223114.
67. Hoang Tran M, Park T, Hur J. Solution-processed ZnO:graphene quantum dot/poly-TPD heterojunction for high-performance UV photodetectors. Appl. Surf. Sci. 2021;539:148222.
68. Chang SJ, Duan BG, Hsiao CH, Young SJ, Wang BC, Kao TH, et al. Low-frequency noise characteristics of in-doped ZnO ultraviolet photodetectors. IEEE Photonics Technol. Lett. 2013;25:2043–46.
69. Rajab FH, Taha RM, Hadi AA, Khashan KS, Mahdi RO. Laser induced hydrothermal growth of ZnO rods for UV detector application. Opt. Quantum Electron. 2023;55:208.
70. Agarwal L, Tripathi S. High responsivity ZnO based p-n homojunction UV-photodetector with series Schottky barrier. Semicond. Sci. Technol. 2020;35:065001.
71. Al-Hardan NH, Jalar A, Abdul Hamid MA, Keng LK, Ahmed NM, Shamsudin R. A wide-band UV photodiode based

on *n*-ZnO/p-Si heterojunctions. Sensors Actuators A Phys. 2014;207:61–66.
72. Ali GM. Performance analysis of planar Schottky photodiode based on nanostructured ZnO thin film grown by three different techniques J. Alloys Compd. 2020;831:154859.
73. Hussain I, Soomro MY, Bano N, Nur O, Willander M. Interface trap characterization and electrical properties of Au-ZnO nanorod Schottky diodes by conductance and capacitance methods. J. Appl. Phys. 2012;112:064506.
74. Moloi SJ, Bodunrin JO. Characterisation of interface states of Al/p-Si Schottky diode by current–voltage and capacitance–voltage–frequency measurements. J. Mater. Sci. Mater. Electron. 2023;34:1712.
75. Orak I, Kocyigit A, Karteri İ, Uruş S. Frequency-dependent electrical characterization of GO-SiO_2 composites in a Schottky device. J. Electron. Mater. 2018;47:6691–700.
76. Azizian-Kalandaragh Y, Badali Y, Jamshidi-Ghozlu M-A, Hanife F, Özçelik S, Altındal Ş, et al. The temperature-dependent dielectric properties of the Au/ZnO-PVA/n-Si structure. Phys. B Condens. Matter. 2023;650:414495.
77. Tan SO, Tecimer HU, Çiçek O, Tecimer H, Altındal Ş. Frequency dependent C–V and G/ω–V characteristics on the illumination-induced Au/ZnO/n-GaAs Schottky barrier diodes. J. Mater. Sci. Mater. Electron. 2017;28:4951–57.
78. Nikravan A, Badali Y, Altındal Ş, Uslu İ, Orak İ. On the frequency and voltage-dependent profiles of the surface states and series resistance of Au/ZnO/n-Si structures in a wide range of frequency and voltage. J. Electron. Mater. 2017;46:5728–36.
79. Bengi S, Çetinkaya HG, Altındal Ş, Zeyrek S. Examination of electrical and dielectric parameters of Au/n-Si Schottky barrier diodes (SBDs) with organic perylene interlayer using impedance measurements under various illumination intensities. J. Electron. Mater. 2024;53:5606–16.
80. Kanbur H, Altındal Ş, Tataroğlu A. The effect of interface states, excess capacitance and series resistance in the Al/SiO_2/p-Si Schottky diodes. Appl. Surf. Sci. 2005;252:1732–38.
81. Güçlü ÇŞ, Tanrıkulu EE, Ulusoy M, Kalandargh YA, Altındal Ş. Frequency-dependent physical parameters, the voltage-dependent profile of surface traps, and their lifetime of Au/(ZnCdS-GO:PVP)/n-Si structures by using the conductance method. J. Mater. Sci. Mater. Electron. 2024;35:348.
82. Çetinkaya HG, Bengi S, Sevgili O, Altındal Ş. The capacitance/conductance and surface state intensity characteristics of the Al/(CMAT)/p-Si structures. Phys. Scr. 2024;99:025955.
83. Elgazzar E, Tataroğlu A, Al-Ghamdi AA, Al-Turki Y, Farooq WA, El-Tantawy F. Thermal sensors based on delafossite film/p-silicon diode for low-temperature measurements. Appl. Phys. A. 2016;122:617.
84. Yıldırım M, Kocyigit A. Characterization of Al/In:ZnO/p-Si photodiodes for various In doped level to ZnO interfacial layers. J. Alloys Compd. 2018;768:1064–75.
85. Bengi S, Çetinkaya HG, Altındal Ş, Durmuş P. Investigation of the frequency effect on electrical modulus and dielectric properties of Al/p-Si structure with %0.5 Bi:ZnO interfacial layer. Ionics (Kiel). 2024;30:3651–59.
86. Badali Y, Altındal Ş, Uslu İ. Dielectric properties, electrical modulus and current transport mechanisms of Au/ZnO/n-Si structures. Prog. Nat. Sci. Mater. Int. 2018;28:325–31.
87. Erdal MO, Kocyigit A, Yıldırım M. The rate of Cu doped TiO_2 interlayer effects on the electrical characteristics of Al/Cu:TiO_2/n-Si (MOS) capacitors depend on frequency and voltage. Microelectron. Reliab. 2020;106:113591.

How to cite this article: Erkol M, Coşkun M, Coşkun FM, Kocyigit A. The light detection performance of ZnO-based Schottky-type photodetector as a function of changing solution molarity. J Am Ceram Soc. 2025;108:e20343. https://doi.org/10.1111/jace.20343